

Independent Regulation of Basal Neurotransmitter Release Efficacy by Variable Ca^{2+} Influx and Bouton Size at Small Central Synapses

Yaroslav S. Ermolyuk, Felicity G. Alder, Christian Henneberger[‡], Dmitri A. Rusakov, Dimitri M. Kullmann, Kirill E. Volynski*

UCL Institute of Neurology, University College London, United Kingdom

Abstract

The efficacy of action potential evoked neurotransmitter release varies widely even among synapses supplied by the same axon, and the number of release-ready vesicles at each synapse is a major determinant of this heterogeneity. Here we identify a second, equally important, mechanism for release heterogeneity at small hippocampal synapses, the inter-synaptic variation of the exocytosis probability of release-ready vesicles. Using concurrent measurements of vesicular pool sizes, vesicular exocytosis rates, and presynaptic Ca^{2+} dynamics, in the same small hippocampal boutons, we show that the average fusion probability of release-ready vesicles varies among synapses supplied by the same axon with the size of the spike-evoked Ca^{2+} concentration transient. We further show that synapses with a high vesicular release probability exhibit a lower Ca^{2+} cooperativity, arguing that this is a direct consequence of increased Ca^{2+} influx at the active zone. We conclude that variability of neurotransmitter release under basal conditions at small central synapses is accounted for not only by the number of release-ready vesicles, but also by their fusion probabilities, which are set independently of bouton size by variable spike-evoked presynaptic Ca^{2+} influx.

Citation: Ermolyuk YS, Alder FG, Henneberger C, Rusakov DA, Kullmann DM, et al. (2012) Independent Regulation of Basal Neurotransmitter Release Efficacy by Variable Ca^{2+} Influx and Bouton Size at Small Central Synapses. *PLoS Biol* 10(9): e1001396. doi:10.1371/journal.pbio.1001396

Academic Editor: Alberto Bacci, ICM - Institut du Cerveau et de la Moelle épinière Hôpital Pitié-Salpêtrière 47, bd de l'Hôpital, France

Received: May 22, 2012; **Accepted:** August 16, 2012; **Published:** September 25, 2012

Copyright: © 2012 Ermolyuk et al. This is an open-access article distributed under the terms of the Creative Commons Attribution License, which permits unrestricted use, distribution, and reproduction in any medium, provided the original author and source are credited.

Funding: The study was supported by the Medical Research Council United Kingdom (G0600089), the Brain Research Trust, the Wellcome Trust (WT084311), the European Research Council, and a UCL Bridging Award for CH. The funders had no role in study design, data collection and analysis, decision to publish, or preparation of the manuscript.

Competing Interests: The authors have declared that no competing interests exist.

* E-mail: k.volynski@ucl.ac.uk

[‡] Current address: Institute of Cellular Neuroscience, University of Bonn, Bonn, Germany

Abbreviations: AP, action potential; AZ, active zone; CNS, central nervous system; CV, coefficient of variation; RRP, readily releasable pool; ROI, region of interest; SEM, standard error of the mean; SRC1, SynaptoRedC1; TRP, total recycling pool; VGCC, voltage-gated Ca^{2+} channel

Introduction

The probability of neurotransmitter release (P_{rel}) in response to an action potential (AP) determines the efficacy of information transfer at synapses in the brain. Importantly, in the central nervous system (CNS) P_{rel} varies widely even among synapses supplied by a single axon, and this heterogeneity has been attributed in part to a target-specific adjustment of presynaptic properties [1–6]. However, P_{rel} also varies considerably among synaptic boutons contacting the same type of target cell or even the same dendritic branch [2,7–9], and it has been proposed that exocytosis efficacy is adjusted according to the local level of postsynaptic dendritic activity [10]. At present, however, the mechanisms that set the distinct basal release probabilities among individual small central synapses in a population remain largely unknown.

In general, P_{rel} at a given synaptic bouton is determined by the number of vesicles within the readily releasable pool (RRP, vesicles docked at the active zone, AZ [11]) and by the average fusion probability (p_v) of individual RRP vesicles. According to the classical binomial model, the average number of vesicles released in response to a single AP is then $N_{AP} = RRP \cdot p_v$ with a probability

that at least one vesicle is released given by $P_{rel} = 1 - (1 - p_v)^{RRP}$. At small central synapses, both in situ and in neuronal culture, the size of the AZ, the RRP size (RRP), and the total recycling pool (TRP) size (TRP) change together with the size of the presynaptic bouton [12,13]. Thus, in general, P_{rel} is higher at larger synapses and therefore variable presynaptic bouton size is a major determinant of P_{rel} . However, P_{rel} also varies substantially even among synaptic boutons of similar size (e.g., [14–16]). Two principal mechanisms are generally thought to underlie this heterogeneity in P_{rel} . The first is variation in RRP size, due to differences in the density of docked synaptic vesicles at the AZ and/or in the dimensions of the AZ itself [12,16]. The second mechanism that could potentially contribute to variability in P_{rel} is the average fusion probability of individual RRP vesicles p_v , which might vary from synapse to synapse [3]. Although p_v has long been known to follow changes in Ca^{2+} entry at an individual synapse, it is unclear to what extent basal p_v varies among boutons supplied by a given axon. Nor is it known if any systematic relationship exists between p_v and presynaptic bouton size.

To address these fundamental questions, and to understand the relationship between the basic mechanisms that determine heterogeneity of neurotransmitter release, we have developed a

Author Summary

Synaptic transmission underlies information transfer among neurons in the brain. The probability that a synapse will release neurotransmitter in response to an action potential varies widely, even among synapses supplied by the same axon. The molecular mechanisms underlying this heterogeneity remain poorly understood. At the level of single synapses, release efficacy is determined largely by two factors: (i) the number of neurotransmitter-containing vesicles ready to be released, and (ii) by the fusion probabilities of these vesicles. By using novel imaging techniques at individual hippocampal presynaptic boutons in culture, we distinguish two independent sources of variability of release probability in small central synapses. First, we find differences in the number of releasable vesicles, and second, we find differences in the exocytosis probability of individual vesicles. To our knowledge, this is the first direct experimental demonstration that the fusion probability of release-ready vesicles is variable among synapses supplied by a single axon, and contributes roughly as much to the overall variability in release probability as does the number of release-ready vesicles.

suite of imaging methods that allowed us to directly relate presynaptic Ca^{2+} dynamics and vesicular exocytosis at the same small synaptic boutons. By combining fluorescence imaging of vesicular release with fluorescence imaging of presynaptic Ca^{2+} dynamics in cultured hippocampal neurons we have concurrently estimated, at the level of individual synaptic boutons, all the major functional presynaptic parameters including: the overall AP-evoked vesicular release rate R_{rel} , the relative sizes of the RRP and TRP, the average release probability of individual RRP vesicles p_v , the relative bouton size, the total magnitude of presynaptic Ca^{2+} influx, and the relative endogenous Ca^{2+} buffer capacity. By comparing among boutons imaged in parallel, including those supplied by the same axon, we show that R_{rel} , p_v , RRP , TRP , the ratio RRP/TRP , the volume-averaged AP-evoked presynaptic Ca^{2+} concentration transient $\Delta[\text{Ca}^{2+}]_{total}$, and the bouton size, all vary extensively among synapses supplied by a given axon. Whilst our results confirm that both RRP and TRP scale together with bouton size [12,13], we find that p_v and $\Delta[\text{Ca}^{2+}]_{total}$ do not depend on the size of the bouton but correlate tightly with one another. Furthermore, we show that differences in p_v among boutons supplied by the same axon are accounted for by inter-synaptic variability in presynaptic Ca^{2+} influx but not by differences in endogenous Ca^{2+} buffering capacity. Consistent with substantial inter-bouton inhomogeneity of Ca^{2+} influx, we also show that the apparent Ca^{2+} cooperativity of AP-evoked vesicular release is lower at synapses with high p_v . Taken together, our data argue that variable efficacies of AP-evoked neurotransmitter release among small CNS synapses supplied by a given axon are regulated by two independent mechanisms: (i) synaptic bouton size, which primarily affects the RRP size; and (ii) synapse-specific regulation of Ca^{2+} influx at the AZ, which directly determines the average fusion probability of RRP vesicles p_v .

Results

Co-variation of Vesicular Release Rate and AP-Evoked Presynaptic Fluorescence Ca^{2+} Transients among Individual Synapses

A major obstacle to date in relating neurotransmitter release to presynaptic Ca^{2+} dynamics is that they have not been measured

together in the same small CNS synapses. To achieve this we combined two well-characterized fluorescence imaging techniques that have been extensively used in isolation: imaging of vesicular release with styryl FM dyes (e.g., [8,17–19]) and measurements of presynaptic Ca^{2+} dynamics with fluorescent Ca^{2+} indicators (e.g., [20–24]).

Because Ca^{2+} indicators themselves may affect exocytosis [25,26], we measured vesicular release prior to Ca^{2+} indicator loading. We labeled all recycling vesicles with the amphiphilic styryl dye SynaptoRedC1 (SRC1, a less lipophilic analogue of FM 4–64) using several rounds of saturating high-frequency stimulation, and recorded the SRC1 de-staining time course in individual boutons over a large area containing 300–500 putative synapses, first at rest and then during low-frequency (0.5-Hz) stimulation (Methods and Figure 1A–1C and 1E).

The SRC1 de-staining kinetics in individual boutons were well approximated by mono-exponential functions (Figure 1F). In agreement with previous reports (e.g., [14,27]) both the spontaneous SRC1 de-staining rate determined in the absence of stimulation k_{sp} , and the SRC1 de-staining rate during the 0.5-Hz AP train (k_{ev}) varied extensively among boutons. Furthermore, on average k_{ev} was ~ 6 – 7 -fold higher than k_{sp} (Figure S1A and S1B). Although k_{sp} provides a measure of spontaneous exocytosis, both k_{sp} and k_{ev} are also affected by non-specific loss of SRC1 fluorescence. To correct for these factors we calculated the specific AP-evoked SRC1 de-staining rate as $k_{AP} = k_{ev} - k_{sp}$. At each recorded bouton we also estimated the relative size of the TRP of vesicles as proportional to the total specific SRC1 fluorescence loss ($\Delta F_{FMtotal}$) during the de-staining experiment. This was measured by calculating the difference between SRC1 fluorescence immediately after the dye washout and the residual (background) fluorescence after a series of high-frequency stimulus trains designed to release all recycling vesicles (Methods; Figure 1A). These measurements allowed us to compare AP-evoked vesicular release among individual synaptic boutons. Indeed, the specific AP-evoked vesicular release rate could be obtained from $R_{rel} = [k_{AP} \cdot \Delta F_{FMtotal}] / v$ (where $v = 0.5$ Hz is the stimulation frequency). This measure is proportional to the average number of vesicles released by a single AP, and thus closely related to P_{rel} (see Discussion).

Next, we aimed to relate R_{rel} to presynaptic Ca^{2+} dynamics measured in a subset of boutons supplied by a single presynaptic neuron. To achieve this we re-loaded synaptic vesicles with SRC1 to visualize the synapses once again, and filled a nearby neuron with the high-affinity fluorescent Ca^{2+} indicator Fluo-4 together with the morphological tracer Alexa Fluor 568 via a somatic patch pipette in whole-cell mode (Methods). In approximately 5% of cases the axon of the patched cell could be traced into the area where exocytosis had previously been documented, and a subset of boutons supplied by the same axon could be identified unambiguously (Figure 1D). We then recorded presynaptic Ca^{2+} fluorescence transients in these boutons (using a 500-Hz line-scan), evoked by a single AP followed by a 100-Hz AP train (Figure 1E) to record the saturating (maximal) fluorescence of Fluo-4 [21,22]. After subtracting the background fluorescence for each recording sweep we determined the following parameters: the resting fluorescence F_0 , the AP-evoked fluorescence increment ΔF (integrated over 10 ms), and the maximal Fluo-4 fluorescence F_m (Figure 1G). To compare the magnitudes of AP-evoked presynaptic Ca^{2+} transients among individual boutons we used the ratio $\Delta F/F_m$. This allowed us to compare the amplitudes of presynaptic Ca^{2+} influx without making any assumptions about resting Ca^{2+} levels [22].

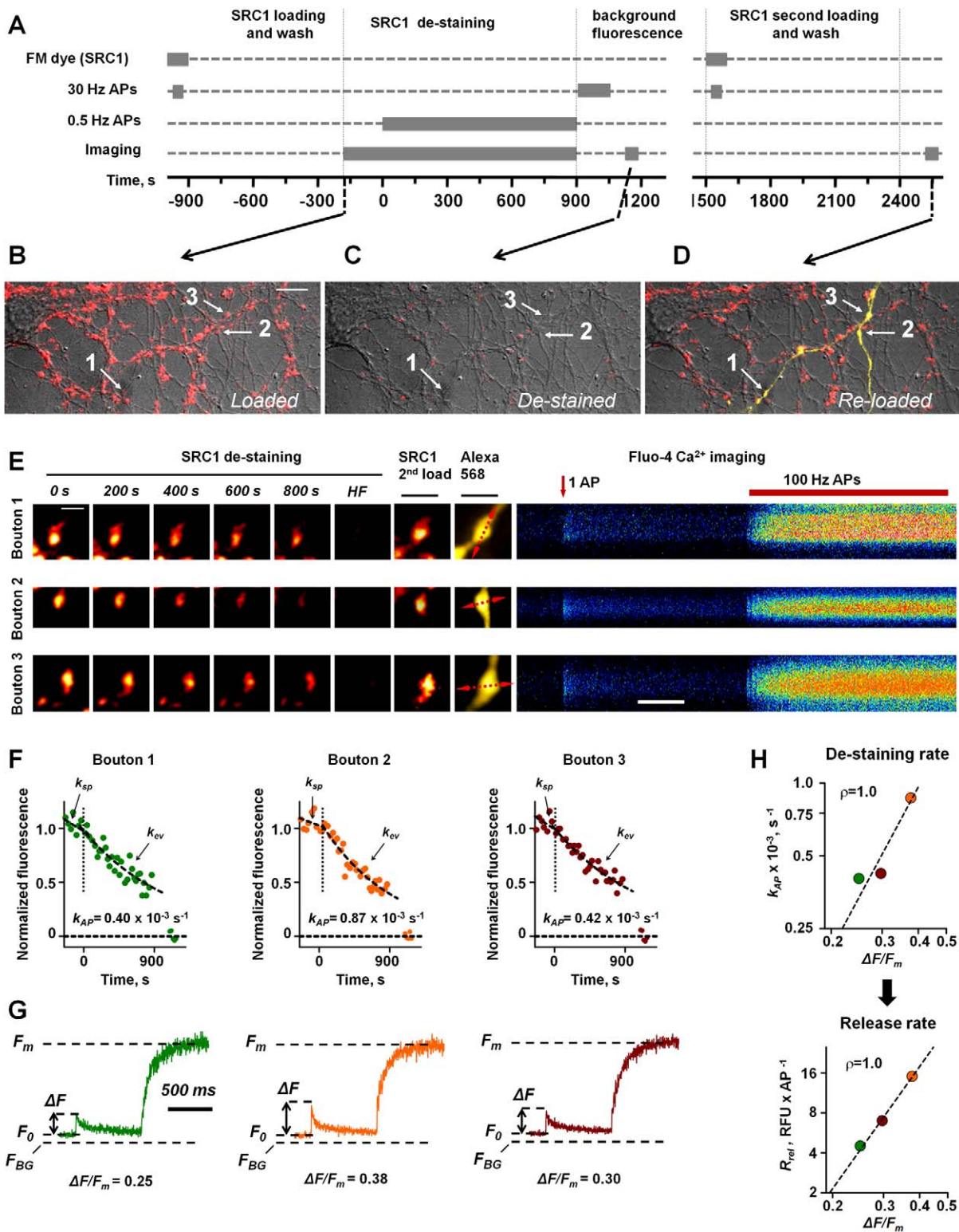


Figure 1. Consecutive imaging of vesicular exocytosis and presynaptic Ca²⁺ dynamics in individual synaptic boutons supplied by the same axon. (A) Experimental paradigm (sequence of loading and imaging protocols) and (B–H) a detailed illustration of a typical experiment. (B,C) Cultured hippocampal neurons (DIC and fluorescence images) showing SRC1 staining (red) before (B) and after (C) the de-staining experiment. (D) The area shown in (B) and (C), imaged after (i) re-staining with SRC1 and (ii) whole-cell patch-loading of a presynaptic cell with Fluo-4 and Alexa Fluor 568 (yellow). A single axon with two branches is clearly seen. Arrows in (B–D) depict boutons (1, 2, and 3) in which both SRC1 de-staining and Ca²⁺ dynamics have been recorded. (E) Details of SRC1 and Fluo-4 imaging in individual boutons. Left, SRC1 stained presynaptic boutons during 0.5-Hz stimulation, after the high-frequency (HF) de-staining, and after re-staining with SRC1 and patch-loading with Fluo-4 and Alexa Fluor 568. Line-scan positions used for Ca²⁺ recordings are shown with red dotted lines on the Alexa image. Right, line-scan recordings of Ca²⁺ responses in selected boutons; brightness is color-coded, red arrow, single spike onset; red segment above, a saturating 100-Hz train of APs. (F) Analysis of SRC1 de-staining

in recorded boutons; fluorescence traces were normalized to the initial SRC1 fluorescence at the beginning of 0.5-Hz stimulation (marked by dotted vertical lines), dashed lines depict single-exponent fits in the absence of stimulation (k_{sp}) and during 0.5-Hz stimulation (k_{ev}). The specific AP-evoked de-staining rate in each bouton was calculated as $k_{AP} = k_{ev} - k_{sp}$. (G) Analysis of presynaptic Ca^{2+} dynamics in recorded boutons. Line-scan fluorescence time courses corresponding to stimulation paradigms shown in (E), average of five traces. Dashed lines: maximal value of Fluo-4 fluorescence F_m , resting Ca^{2+} fluorescence F_0 , background fluorescence F_{BG} , and peak amplitude of AP-evoked fluorescence integrated over 10 ms ΔF . (H) AP-evoked SRC1 de-staining rate k_{AP} (top) and vesicular release rate R_{rel} (bottom) plotted against the amplitude of AP-evoked presynaptic Ca^{2+} fluorescence $\Delta F/F_m$. Boutons are color coded as in (F) and (G). RFU, relative fluorescence units. Spearman rank correlation coefficients ρ are indicated. Dashed lines show data fits with a power function. Scale bars, 10 μm (B), 2 μm (E, top left), and 200 ms (E, bottom right). doi:10.1371/journal.pbio.1001396.g001

We used this protocol to measure concurrently vesicular release rates and presynaptic Ca^{2+} dynamics in two to five individual boutons supplied by the same axon (Figures 1H and S1A). Importantly, we found that in all experiments, both the AP-evoked SRC1 de-staining rate k_{AP} , and the release rate R_{rel} , were positively correlated with the magnitude of the AP-evoked presynaptic Ca^{2+} fluorescence transient $\Delta F/F_m$ ($n = 6$ independent experiments, Figures 1H and S1).

In addition to the magnitude of AP-evoked Ca^{2+} influx itself, the absolute value $\Delta F/F_m$ is also determined by several other factors including the concentration of endogenous Ca^{2+} buffers and the equilibrated concentration of Fluo-4 in the axon [22]. These parameters may vary among different neurons ([28]; see also Figure S5A). Therefore, to combine data from boutons supplied by different axons across experiments we normalized $\Delta F/F_m$, k_{AP} , and R_{rel} to the respective mean values in each individual cell: this normalization standardized the value range among boutons recorded in different neurons and further revealed a tight correlation between the vesicular release rate and $\Delta F/F_m$ signal (Figure 2).

Which Mechanisms Could Account for the Correlation between $\Delta F/F_m$ and Vesicular Exocytosis Rate?

We next asked what possible mechanisms could explain this result. The experimentally measured vesicular release rate R_{rel} is proportional to the average number of vesicles released per AP, and therefore depends on both RRP size and p_v : $R_{rel} \propto RRP \cdot p_v$. Thus the data reported above could be explained by co-variation of RRP or p_v , or both, with the volume-averaged AP-evoked Ca^{2+} fluorescence signal $\Delta F/F_m$.

Synaptic vesicular release is triggered by voltage-gated Ca^{2+} channels (VGCCs) that are located at the AZ in the immediate

vicinity of docked RRP vesicles (for review see [29,30]). Furthermore, accumulating functional and ultrastructural data show that VGCCs are enriched in the AZ [16,31–36] where they compete to occupy specific presynaptic “slots” [37,38] (although see [39]), which may be in a fixed stoichiometric relationship with vesicle docking sites. Therefore, it is possible that the correlation between vesicular release rates and the volume-averaged amplitude of AP-evoked presynaptic Ca^{2+} transient simply reflects inter-synaptic variability in the relative size of the AZ and/or RRP [16]. Indeed, if one of two synapses of equal volume has a larger AZ, we would expect it also to have more RRP vesicles and also more VGCCs, and therefore a higher R_{rel} and $\Delta F/F_m$. Alternatively, the tight correlation between R_{rel} and $\Delta F/F_m$ may principally reflect a different mechanism—inter-synaptic heterogeneity of AP-evoked presynaptic Ca^{2+} influx at the vesicular release sites. In this case p_v (and as a consequence R_{rel}) should also vary with the amplitude of the Ca^{2+} fluorescence transient.

The Average Release Probability of Individual RRP Vesicles p_v Varies Extensively among Synaptic Boutons Supplied by the Same Axon

To distinguish between these two possibilities it is necessary to compare p_v values among individual synaptic boutons supplied by the same axon. The binomial model of vesicular release (e.g., refs. [40,41]) gives a simple expression for the SRC1 de-staining rate evoked by low-frequency AP-trains (k_{AP}), as a function of the ratio of RRP to TRP vesicular pool sizes and p_v : $k_{AP} = v \cdot [RRP/TRP] p_v$ (Text S1). Therefore, to estimate p_v we sequentially determined the RRP/TRP ratio and k_{AP} in the same boutons.

The detailed experimental protocol is outlined in Figure 3A. To identify synaptic boutons supplied by a single axon we first patch-loaded a neuron in the field of view with the morphological tracer Alexa Fluo 568 (Figure 3B). After withdrawal of the patch-pipette we fully labeled the TRP of vesicles in all synapses in the field of view using saturating high-frequency field stimulation (Methods). The relative RRP size can be estimated by measuring the SRC1 fluorescence decrease evoked by brief high-frequency trains of APs that are designed to completely deplete the RRP [19,42–44]. We therefore modified the classical SRC1 de-staining experiment: in addition to measuring k_{AP} and the total specific SRC1 fluorescence loss $\Delta F_{FMtotal}$ (which is proportional to the TRP size), we also measured the SRC1 fluorescence drop caused by a 30-Hz train of 60 APs $\Delta F_{FM(60APs)}$ (which is proportional to the RRP size). This allowed us to estimate the RRP/TRP ratio as $[\Delta F_{FM(60APs)}/\Delta F_{FMtotal}]/\varphi$ (where $\varphi = 2.74$ is a scaling coefficient) (see Text S2). Finally, we allowed the remaining SRC1-labeled vesicles to re-equilibrate between TRP and RRP for a further 5–7 min [19] and then measured k_{AP} using 0.5-Hz stimulation as before (Figure 3C).

From the data thus obtained, k_{AP} , the RRP/TRP ratio, the relative RRP and TRP sizes, and the vesicular release rate R_{rel} , all varied extensively, even among synaptic boutons supplied by the same axon (Figures 3D–3F and S4A–S4C). In agreement with

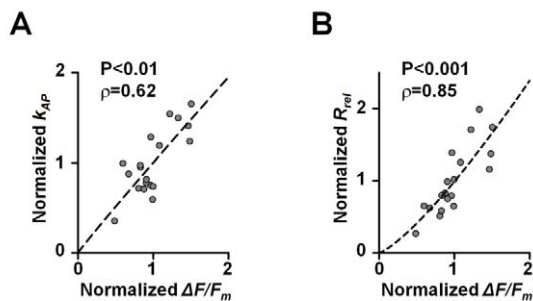


Figure 2. Co-variation of vesicular release rate and AP-evoked presynaptic Ca^{2+} fluorescence transients. Dependencies of AP-evoked SRC1 de-staining rate k_{AP} (A) and vesicular release rate R_{rel} (B) on the amplitude of AP-evoked presynaptic Ca^{2+} fluorescence $\Delta F/F_m$, pooled data from six axons ($n = 19$ boutons). All parameters are normalized to the respective mean value in each experiment (axon), non-normalized data are presented in Figures 1H and S2. Correlation coefficients ρ and significance levels p (Spearman rank correlation test) are indicated. Dashed lines show data fits with a power function. doi:10.1371/journal.pbio.1001396.g002

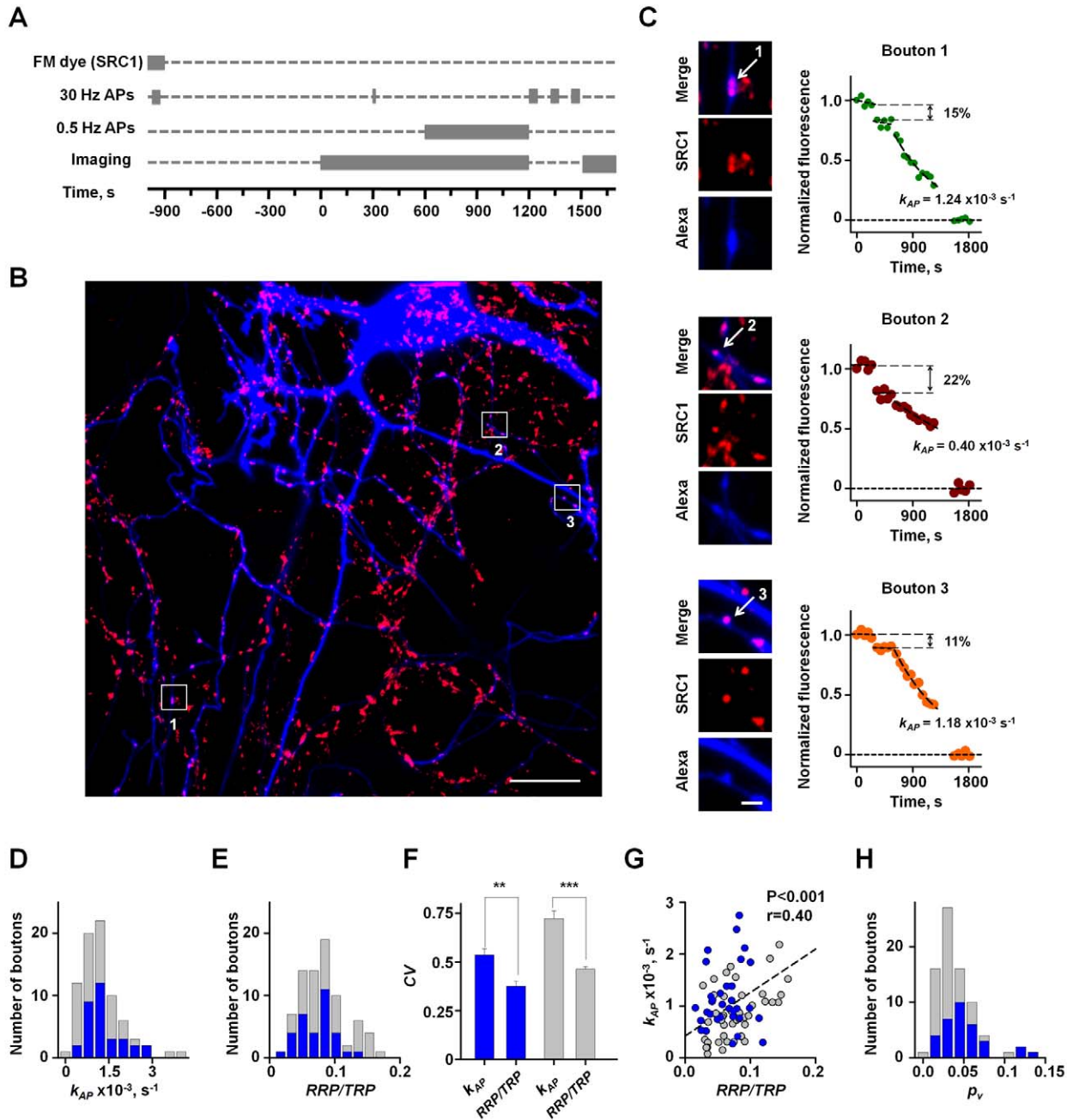


Figure 3. Simultaneous measurements of RRP/TRP ratio and AP-evoked SRC1 de-staining rate k_{AP} demonstrate heterogeneity of p_v among synapses supplied by single axons. (A) Experimental paradigm. A presynaptic cell was filled with the morphological tracer Alexa Fluor 568 using whole-cell patch-clamp. Recycling synaptic vesicles in all boutons in the field of view were labeled with SRC1 using high-frequency field stimulation. After dye washout the RRP/TRP ratio in individual boutons was estimated using 30-Hz 60 AP train (see main text and Text S2 for details). This was followed by measurements of SRC1 de-staining kinetics (k_{AP}) during low-frequency 0.5-Hz stimulation. (B) Fluorescence image from a typical experiment showing SRC1 labeled boutons (red) and axodentritic tree of a single neuron filled with Alexa Fluor 568 (blue). White boxes depict regions of interest containing synaptic boutons analyzed in (C). (C) High resolution images and de-staining profiles in three typical synaptic boutons (depicted by arrows) supplied by the Alexa Fluor 568 loaded neuron. (D and E) Frequency histograms of k_{AP} (D) and RRP/TRP (E) from the experiment illustrated in (B and C). Blue histogram, boutons supplied by the Alexa loaded axon; grey histogram, all boutons in the field of view. (F) Comparison of RRP/TRP and k_{AP} variability. Blue bars, average CVs for RRP/TRP and k_{AP} recorded in synaptic boutons located on single axons; grey bars, average CVs for the same parameters for all boutons recorded in the same experiments. Data are mean \pm standard error of the mean (SEM) from 11 independent experiments, $**p < 0.01$ and $***p < 0.001$, Wilcoxon signed rank test. (G) Relationship between k_{AP} and RRP/TRP . Blue, data points from boutons supplied by the Alexa loaded axon shown in (B); grey data points from all boutons in the field of view. Dotted line shows linear regression for all boutons in the field of view. Pearson's correlation coefficient r and significance levels P (Pearson product correlation test) are indicated. (H) Frequency histogram of p_v , calculated for the same set of boutons as in (D, E, and G) using $p_v = k_{AP}/[RRP/TRP]$. Scale bars 20 μm (B) and 2 μm (C).

doi:10.1371/journal.pbio.1001396.g003

previous reports [45], RRP size correlated with the TRP size (Figure S4D), whereas the RRP/TRP ratio was independent of the TRP size (Figure S4E). Surprisingly, even though k_{AP} should be directly proportional to the RRP/TRP ratio, there was only a weak correlation between these parameters (e.g., Figure 3G). Indeed, some boutons with relatively low RRP/TRP had a high AP-dependent de-staining rate (e.g., boutons 1 and 3) (Figure 3C), while other boutons with a large RRP/TRP could have a relatively slow k_{AP} (e.g., bouton 2). Moreover, in each experiment the coefficient of variation (CV) of k_{AP} was always significantly higher than the CV of RRP/TRP (Figure 3F). These results argue that the average fusion probability of RRP vesicles varies extensively among synapses supplied by a given axon. Indeed, by estimating p_v in individual synaptic boutons from $p_v = k_{AP}/[RRP/TRP]$ we found that the average CV of p_v in boutons supplied by single axons was 0.65 ± 0.05 ($n = 11$ axons, on average 16 recorded boutons/axon). Importantly the average value of p_v , measured across all boutons (0.040 ± 0.006) was consistent with previous estimates obtained with complementary methods [13].

Thus, we conclude that the heterogeneity of overall neurotransmitter release probability P_{rel} among synapses supplied by a single axon is determined not only by variability in RRP size [8,11–13] but also by inter-synaptic variability in the average release probability of RRP vesicles p_v .

p_v Varies among Synapses with AP-Evoked Presynaptic Ca^{2+} Fluorescence Response

How does the bouton-to-bouton variability in p_v relate to differences in presynaptic Ca^{2+} dynamics? Upon completion of the SRC1 de-staining experiment we re-patched the identified neuron, loaded it with Fluo-4 and Alexa Fluor 568, and recorded presynaptic Ca^{2+} fluorescence transients in a subset of the same boutons (Figure 4). In the earlier experiments (Figure 1) we measured presynaptic Ca^{2+} dynamics in response to single APs, whilst vesicular release rates were measured during 0.5-Hz stimulation. To match the SRC1 de-staining protocol, in this set of experiments we also measured presynaptic Ca^{2+} dynamics with 0.5-Hz stimulation. For each bouton we recorded the Ca^{2+} fluorescence during a single sweep consisting of five APs delivered at 0.5 Hz followed by a saturating 100-Hz train of 100 APs. To minimise photobleaching and phototoxicity the laser was turned on only during 100-ms periods synchronized with stimulation (Figure 4B).

Consistent with the results reported in Figure 1E and 1G, the 2-s inter-pulse interval was sufficient for the Ca^{2+} fluorescence to return to its resting level (Figure 4C). Although the peak amplitude of the AP-evoked Ca^{2+} fluorescence response exhibited some variability (e.g., Figure 4C, $CV_{fluc} = 0.17 \pm 0.01$, 42 boutons from ten independent experiments), there was no systematic increase or decrease of $\Delta F/F_m$ during the 0.5-Hz stimulation train (Figure 4D). Our measurements of presynaptic Ca^{2+} dynamics can therefore be directly related to measurements of vesicular release rates at the same stimulation frequency. The mean $\Delta F/F_m$ value calculated for all 42 boutons recorded in ten experiments was 0.34 ± 0.02 . Importantly, we observed a substantial variability in presynaptic Ca^{2+} transients among individual boutons supplied by the same neuron ($CV_{axon} = 0.21 \pm 0.03$). This heterogeneity could not be explained by trial-to-trial fluctuations of $\Delta F/F_m$ because averaging of five trials in each bouton restricted this source of variance to only $CV_{fluc}/\sqrt{5} = 0.075$, and therefore the true biological variability of presynaptic Ca^{2+} responses, expressed as CV, was $\sqrt{CV_{axon}^2 - CV_{fluc}^2/5} = 0.20$.

We next related $\Delta F/F_m$ to k_{AP} , RRP/TRP , and p_v measured in the same synapses. Again we found a positive correlation between k_{AP} and the magnitude of AP-evoked presynaptic Ca^{2+} influx $\Delta F/F_m$ (Figure 4E, pooled data from 42 boutons supplied by ten axons). Interestingly we also found that, whilst p_v was strongly correlated with $\Delta F/F_m$ (Figure 4F), the RRP/TRP ratio did not depend on presynaptic Ca^{2+} influx (Figure 4G). Thus, these data argue that co-variation of vesicular release rate and AP-evoked Ca^{2+} fluorescence signal is a consequence of a steep dependence of the average fusion probability of release-ready vesicles on the size of the Ca^{2+} concentration transient.

Inter-synaptic Differences in Bouton Size or Endogenous Ca^{2+} Buffering Capacity Cannot Account for Co-variation of p_v and $\Delta F/F_m$

The volume-averaged amplitude of the AP-evoked presynaptic Ca^{2+} fluorescence response $\Delta F/F_m$ depends on three main factors: the total magnitude of presynaptic Ca^{2+} influx, the concentration and properties of endogenous presynaptic Ca^{2+} buffers, and the bouton volume. Which of these accounts for the co-variation of p_v and $\Delta F/F_m$?

We first estimated the relative volume of each synaptic bouton (V) from the Alexa Fluor 568 fluorescence (Methods; Figure S5). Consistent with electron microscopy data [11–13] we found that both relative RRP and TRP sizes were positively correlated with the bouton volume (Figure 5A and 5B). In contrast, we found no relation between the bouton volume and $\Delta F/F_m$, k_{AP} , RRP/TRP , or p_v (Figure 5C–5F). Therefore, the co-variation of p_v and $\Delta F/F_m$ cannot be explained by the synaptic bouton volume determining both the Ca^{2+} concentration transient and the average release probability of individual RRP vesicles.

We next compared endogenous Ca^{2+} buffering among boutons supplied by the same axon. The classical steady state approximation of the single-compartment model, which is commonly used for small boutons, assumes an equilibrium between Ca^{2+} indicators and endogenous buffers, and predicts that AP-evoked Ca^{2+} transients follow a mono-exponential decay whose rate is decreased by endogenous Ca^{2+} buffers [46–49]. However, consistent with previous reports [20,21,28], we found that presynaptic Ca^{2+} fluorescence transients deviated significantly from a simple mono-exponential relaxation (Figure 1G). Most likely this was because Ca^{2+} indicators and endogenous Ca^{2+} buffers were not at equilibrium during the initial fast phase of the AP-evoked Ca^{2+} fluorescence transient [21].

To compare Ca^{2+} buffering among different boutons without making any steady-state approximations we performed a numerical analysis of presynaptic Ca^{2+} dynamics using a non-stationary single compartment model [21,24] (Text S3). We considered the effect of two major neuronal Ca^{2+} buffers, calbindin-D_{28K} and parvalbumin, on the peak amplitude $\Delta F/F_m$ and on the shape of presynaptic Ca^{2+} Fluo-4 fluorescence transients (Figure 6A–6D). Within a physiological concentration range [28,50] we found that the fast Ca^{2+} buffer calbindin-D_{28K} and the slow Ca^{2+} buffer parvalbumin have only limited effects on the peak amplitude of $\Delta F/F_m$ (Figure 6A and 6C; $\sim 25\%$ reduction for 300 μM calbindin-D_{28K}, and $\sim 10\%$ reduction for 300 μM parvalbumin). Moreover, in agreement with the experimental data (Figure 1G), Ca^{2+} fluorescence traces obtained using the non-stationary model were better described by the sum of two mono-exponential functions (τ_{fast} and τ_{slow}). In contrast to the steady state approximation, the non-stationary model further predicts that endogenous Ca^{2+} buffers should first accelerate and then slow down the AP-evoked Ca^{2+} fluorescence transients (Figure 6A and 6C; see also Discussion).

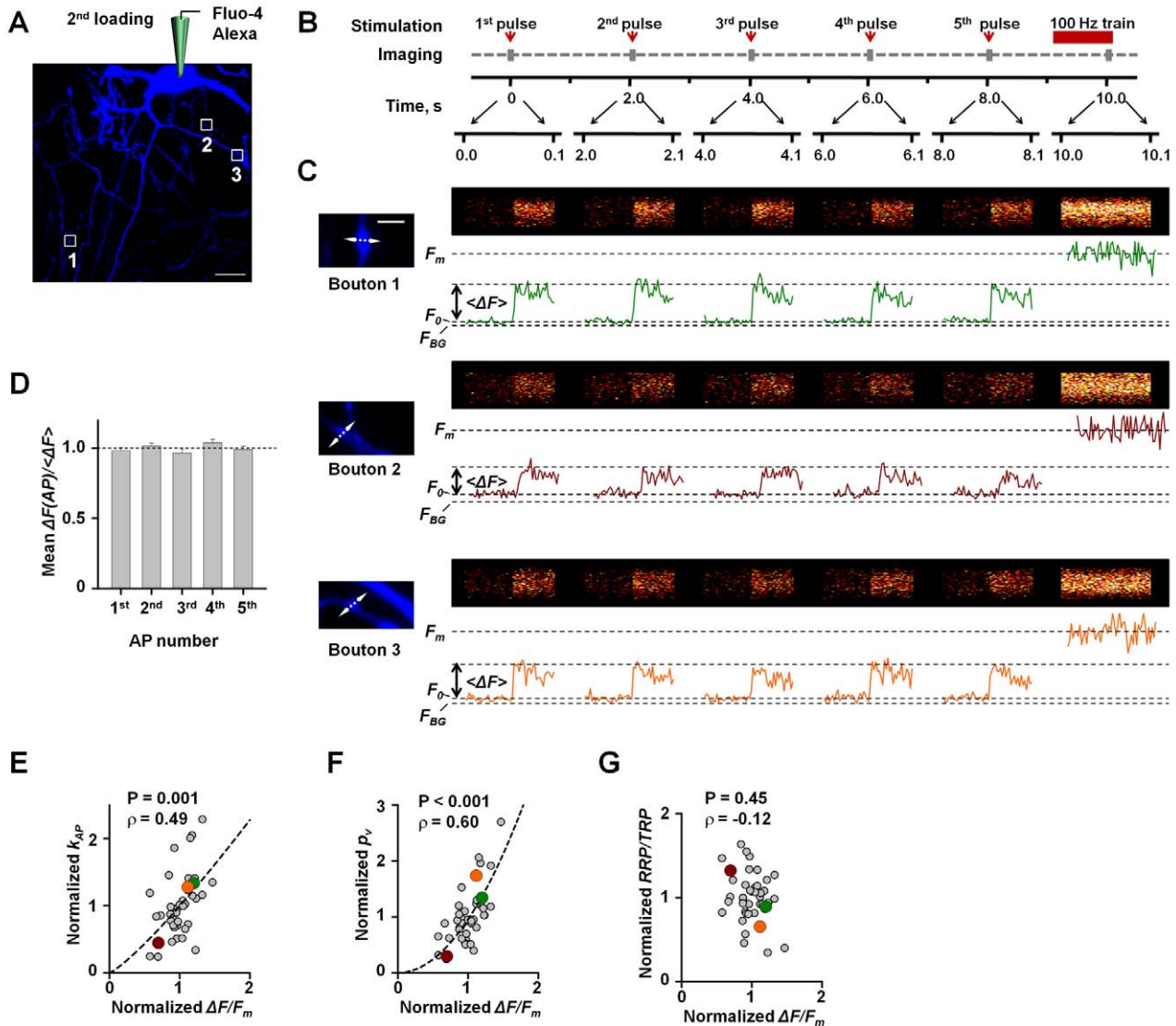


Figure 4. Co-variation of p_v and volume averaged AP-evoked presynaptic Ca^{2+} fluorescent transient. (A) Fluorescence image (Alexa channel) of the same neuron as in Figure 3B after completion of the SRC1 de-staining experiment and subsequent re-patch-loading with Fluo-4 and Alexa Fluor 568. (B) Experimental paradigm. Ca^{2+} fluorescence responses in each bouton were recorded during a single sweep consisting of five APs delivered at 0.5 Hz followed by a saturating 100-Hz train of APs. The laser was turned on only during 100-ms intervals synchronized with single AP stimulation (brown arrows) and at the very end of the 100-Hz 100 AP train (brown horizontal bar) when Fluo-4 signal was already saturated (e.g., Figure 1G). (C) Line-scan recordings of Ca^{2+} dynamics in three typical boutons (prior to these recordings vesicular release in these boutons was measured as illustrated in Figure 3C). The morphology of each bouton (Alexa channel) and the position of line scans are shown on the left. The aspect ratio in line-scan images has been adjusted to optimize figure layout. (D) Amplitude of AP-evoked presynaptic Ca^{2+} influx does not change during 0.5-Hz stimulation. In each recorded bouton Ca^{2+} fluorescence response at every AP of the 0.5-Hz train ($\Delta F(AP)$) was normalized to the average amplitude calculated for all five APs ($\langle \Delta F \rangle$) in the same train. The bars are the mean \pm SEM values of $\Delta F(AP)/\langle \Delta F \rangle$ in all recorded boutons ($n = 42$ from ten independent experiments). $\Delta F(AP)/\langle \Delta F \rangle$ did not vary systematically with the AP number ($p = 0.2$, one-way ANOVA). (E–G) AP-evoked SRC1 de-staining rate k_{AP} (D), the average release probability of individual RRP vesicles p_v (E), and the RRP/TRP ratio (F), plotted against the amplitude of AP-evoked presynaptic Ca^{2+} fluorescence $\Delta F/F_m$. All parameters are normalized to the respective mean value in each experiment ($n = 42$ boutons from ten independent experiments). Correlation coefficients ρ and significance levels p (Spearman rank correlation test) are indicated. Dashed lines show data fits with a power function. Color-coded data points correspond to boutons 1, 2, and 3 from the experiment analyzed in (C) and also in Figure 3B and 3C. Scale bars 20 μm (A) and 2 μm (C). doi:10.1371/journal.pbio.1001396.g004

We then used the non-stationary model to determine which parameters of Ca^{2+} fluorescence kinetics are specifically sensitive to endogenous Ca^{2+} buffering. The Ca^{2+} buffer concentration affects the fast decay time constant τ_{fast} to a much greater extent than the peak amplitude $\Delta F/F_m$ (Figure 6B and 6D). We therefore compared the shapes of the presynaptic Ca^{2+} fluorescence transients during the first 50 ms after the AP and found that they

were very similar among boutons supplied by single axons (Figures 6E–6G and S6). Moreover, the Ca^{2+} fluorescence time course did not depend on the peak amplitude $\Delta F/F_m$ (Figure 6H). We therefore conclude that the observed variability in $\Delta F/F_m$ among boutons supplied by the same axon cannot be explained by differences in endogenous Ca^{2+} buffering capacity. Instead, the steep correlation between pool p_v and $\Delta F/F_m$ most likely reflects

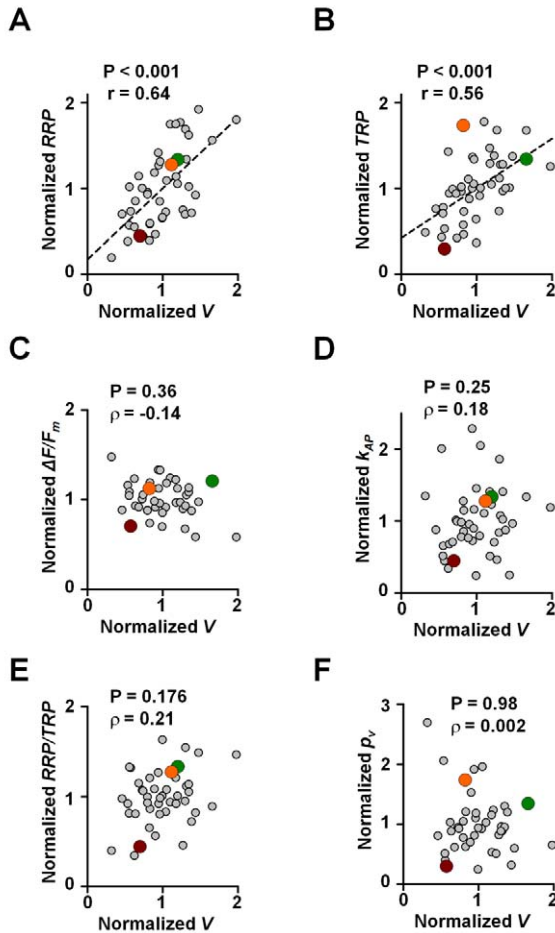


Figure 5. Relationships between functional presynaptic parameters and bouton size. Dependency of normalized RRP size (A), TRP size (B), AP-evoked Ca^{2+} fluorescence step $\Delta F/F_m$ (C), AP-evoked SRC1 de-staining rate k_{AP} (D), the ratio RRP/TRP (E), and the average release of individual RRP vesicles p_v (F) on the normalized synaptic bouton volume V , estimated as proportional to the integral Alexa Fluor 568 fluorescence in each bouton (Figure S5C). Data are from the same set of experiments as in Figure 4E–4G ($n=42$ boutons recorded in ten axons). All parameters are normalized to the respective mean value in each axon. Correlation coefficients ρ and significance levels p (Spearman rank correlation test) are indicated. Dashed lines in (A) and (B) show linear regression. Color-coded data points correspond to boutons 1, 2, and 3 from the experiment illustrated in Figures 3C and 4C. Consistent with previous reports [13] RRP size (A) and TRP size (B) increased with the synaptic bouton volume. In contrast $\Delta F/F_m$ (C), k_{AP} (D), RRP/TRP (E), and p_v (F) did not systematically change with the synaptic bouton size.
doi:10.1371/journal.pbio.1001396.g005

inter-synaptic differences in the magnitude of the volume-averaged AP-evoked presynaptic Ca^{2+} influx.

$\Delta F/F_m$ Provides a Linear Readout of Presynaptic Ca^{2+} Influx

Hitherto we have assumed that $\Delta F/F_m$ provides an unbiased estimate of AP-evoked Ca^{2+} influx. What is the exact relationship between the amplitude of the presynaptic Ca^{2+} fluorescence transient measured with the high affinity indicator Fluo-4 and the total magnitude of AP-evoked presynaptic Ca^{2+} influx (i.e. AP-evoked change of total intracellular Ca^{2+} concentration $\Delta[\text{Ca}^{2+}]_{total}$)? Within the relevant range of $\Delta F/F_m$ (0.1–0.6) the

non-stationary single compartment model predicts a near-linear relationship between $\Delta F/F_m$ and $\Delta[\text{Ca}^{2+}]_{total}$ (Figure S7). To test this prediction experimentally we compared the relative changes in $\Delta F/F_m$ caused by altering the extracellular Ca^{2+} concentration ($[\text{Ca}^{2+}]_{ext}$) among individual synaptic boutons (Figure 7). Elevation of $[\text{Ca}^{2+}]_{ext}$ should increase presynaptic Ca^{2+} influx uniformly at all recorded boutons. On the other hand, if Fluo-4 was partially saturated following an AP the relative increase of Ca^{2+} fluorescence should be smaller in boutons with a higher initial $\Delta F/F_m$ value. When $[\text{Ca}^{2+}]_{ext}$ was increased from 1 mM to 2 mM, however, we observed similar proportional increases in $\Delta F/F_m$ irrespective of the starting value: $\Delta F/F_m$ measured at the two concentrations in different boutons fell on a straight line passing through the origin (Figure 7C, slope: 1.33 ± 0.04). Similarly, increasing $[\text{Ca}^{2+}]_{ext}$ from 2 mM to 4 mM also led to similar fractional increases in $\Delta F/F_m$ in all boutons (Figure 7D, slope: 1.38 ± 0.04). We thus observed no evidence for saturation of peak fluorescence signals in our experimental conditions. We also confirmed that a 100-Hz AP train was sufficient to saturate Fluo-4 completely. Indeed, increasing $[\text{Ca}^{2+}]_{ext}$ did not significantly alter the maximal fluorescence F_m even in boutons with low initial Ca^{2+} influx (Figure 7A), further arguing that $\Delta F/F_m$ measured with Fluo-4 provided a linear readout of $\Delta[\text{Ca}^{2+}]_{total}$.

Ca^{2+} Cooperativity of AP-Evoked Vesicular Release Varies among Synapses

The predominant occurrence of VGCCs within the AZ [31,33–35,51] implies that AP-evoked $\Delta[\text{Ca}^{2+}]_{total}$ is directly related to the local Ca^{2+} concentration transients at the vesicular release sites. This further argues that the observed co-variation of p_v and $\Delta[\text{Ca}^{2+}]_{total}$ could be a direct consequence of inter-synaptic heterogeneity of local Ca^{2+} influx at the AZ. To test this prediction we measured vesicular release rates in individual synaptic boutons at 1, 2, and 4 mM $[\text{Ca}^{2+}]_{ext}$. First we calculated the average k_{AP} in all boutons recorded at each $[\text{Ca}^{2+}]_{ext}$. As expected, we observed a steep dependency of the average vesicular release rate on $[\text{Ca}^{2+}]_{ext}$ (Figure 8A). Moreover, in agreement with previous electrophysiological data (e.g., [31,52]), we observed evidence of significant saturation of the Ca^{2+} release sensor at physiological $[\text{Ca}^{2+}]_{ext}$: although increasing $[\text{Ca}^{2+}]_{ext}$ from 1 mM to 2 mM and from 2 mM to 4 mM led to similar increases in presynaptic Ca^{2+} influx $\Delta[\text{Ca}^{2+}]_{total}$ (Figure 7C and 7D), the average k_{AP} was increased ~ 2.0 -fold when $[\text{Ca}^{2+}]_{ext}$ was switched from 1 mM to 2 mM, but only ~ 1.5 -fold when $[\text{Ca}^{2+}]_{ext}$ was changed from 2 mM to 4 mM (Figure 8A).

This result allowed us to make an important prediction: if inter-synaptic differences in p_v are indeed due to variability in Ca^{2+} influx at the AZ, then the Ca^{2+} release sensor should be saturated to a greater extent in synapses with higher p_v . Since k_{AP} is directly proportional to p_v , this means that Ca^{2+} cooperativity of vesicular release should be lower in synapses with fast SRC1 de-staining, and higher in synapses with slow SRC1 de-staining. To test this prediction we plotted the cumulative probability distributions for k_{AP} at each $[\text{Ca}^{2+}]_{ext}$ (Figure 8B) and then calculated the Ca^{2+} dependency of vesicular release rates in synapses with high and low k_{AP} . In full agreement with the above prediction we found a much steeper dependency of vesicular release rates on presynaptic Ca^{2+} influx in synapses with low k_{AP} (Figure 8C).

We also considered an alternative explanation for this result. Although vesicles docked at the same AZ have been reported to exocytose independently of one another [40,41,53], some studies have argued that vesicular release in small central synapses is

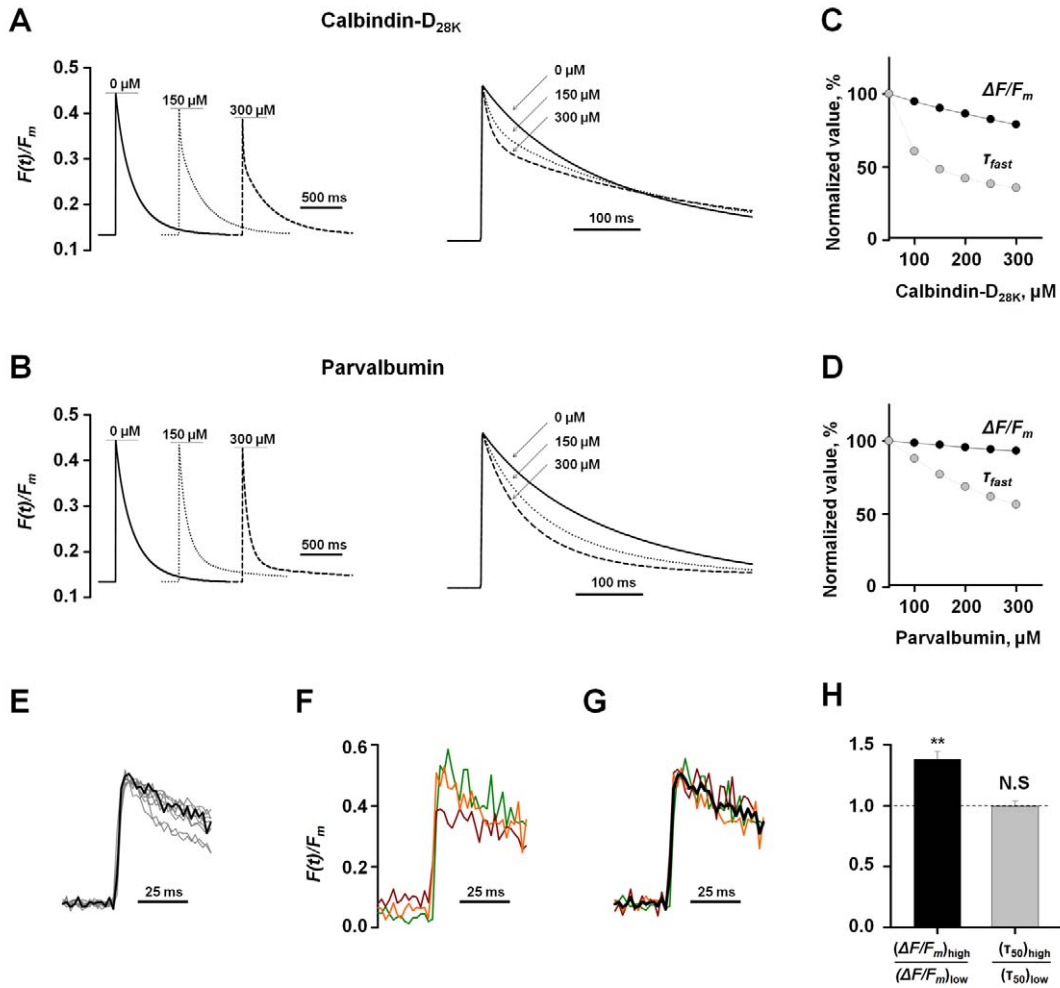


Figure 6. Synaptic boutons located on the same axon have similar endogenous Ca²⁺ buffering capacity. (A, B) Theoretical effects of the major endogenous neuronal Ca²⁺ buffers calbindin-D_{28K} (A) and parvalbumin (B) on presynaptic Ca²⁺ Fluo-4 fluorescence transients calculated using a non-stationary model of presynaptic Ca²⁺ dynamics (Text S3). Left, the effect of increasing concentrations of endogenous Ca²⁺ binding sites on the amplitude and the shape of fluorescence Ca²⁺ transients. Right, peak-scaled Ca²⁺ fluorescence traces illustrating an increase of the fast fluorescence decay component and a decrease of the slow fluorescence decay component with the increase of the endogenous Ca²⁺ buffer concentration. (C, D) Theoretical dependences of changes in the amplitude of AP-evoked Ca²⁺ fluorescence ΔF/F_m (black) and the fast fluorescence decay time constant τ_{fast} (grey) on intracellular concentration of calbindin-D_{28K} (C) and parvalbumin (D): τ_{fast} is more sensitive than ΔF/F_m to changes in endogenous Ca²⁺ buffering. (E) Scaled average responses to a single AP reveal heterogeneity of fast decay rates of Ca²⁺ fluorescence transients recorded in different axons (n = 10 experiments, the same dataset as in Figure 4E–4F). Black trace, the average response recorded in boutons 1, 2, and 3 from experiment illustrated in Figures 3C and 4C. (F, G) Detailed comparison of presynaptic Ca²⁺ dynamics in boutons 1, 2, and 3. (F) Superimposed original traces (color coded as in Figure 4C) showing variability of ΔF/F_m and the resting Ca²⁺ fluorescence F₀ among the three boutons. (G) Scaled responses from the same boutons showing similar fluorescence decay rates (black shows the average of three traces). (H) To test how the fast fluorescence decay rate (τ₅₀, calculated by fitting the Ca²⁺ transient over 50 ms with a mono-exponential function) depends on the amplitude of presynaptic Ca²⁺ fluorescence transient, boutons recorded in each axon were divided into two groups according to the ΔF/F_m value: above the median (high Ca²⁺) and below the median value (low Ca²⁺). Next, the average amplitude ΔF/F_m and the average τ₅₀ were calculated for each group followed by calculation of (ΔF/F_m)_{high}/(ΔF/F_m)_{low} and (τ₅₀)_{high}/(τ₅₀)_{low}. Because the ratio (τ₅₀)_{high}/(τ₅₀)_{low} was not significantly different from 1 we conclude that fast fluorescence decay rate is the same in boutons with high and low ΔF/F_m. Bars are mean ± SEM; n = 10 experiments, **p < 0.01, non-significant (NS) p = 0.70, Wilcoxon signed rank test for single group median. doi:10.1371/journal.pbio.1001396.g006

restricted to only one vesicle per AZ per AP [7,54]. According to the latter model synapses with high p_v , and as a consequence high k_{AP} , should indeed be less sensitive to changes in $[Ca^{2+}]_{ext}$ [8]. But then k_{AP} should also be considerably lower in larger synaptic boutons, which contain more readily releasable vesicles. However k_{AP} did not vary systematically either with the RRP and TRP size (Figures S1F, S4F and S4G) or with the synaptic bouton size (Figure 5D). Our results therefore argue that the inverse relationship between the AP-evoked SRC1 de-staining rate and

the Ca²⁺ cooperativity of release is a direct consequence of inter-synaptic variability of local Ca²⁺ influx at the AZ.

Discussion

The goal of this study was to understand the major factors underlying heterogeneity of AP-evoked neurotransmitter release at small central synapses. It is commonly accepted that the efficacy of synaptic vesicular release is directly determined by the number of

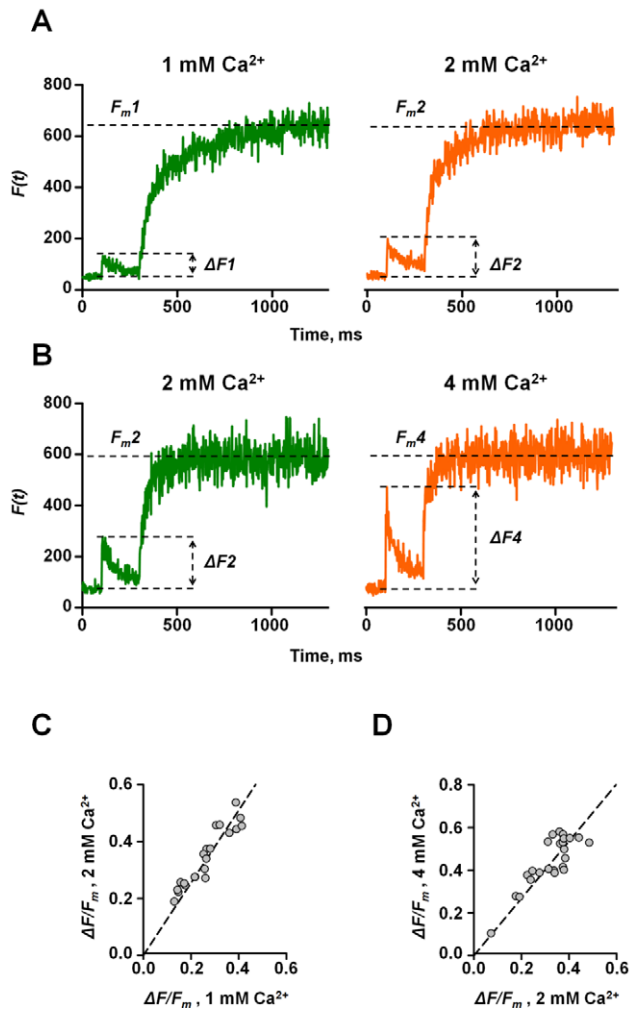


Figure 7. Linear relationship between $\Delta F/F_m$ and total magnitude of presynaptic Ca^{2+} influx. (A, B) Typical Ca^{2+} fluorescence responses to a single AP followed by a saturating train of 100 APs in individual synaptic boutons recorded at two different $[\text{Ca}^{2+}]_{\text{ext}}$: 1 mM and 2 mM (A), and 2 mM and 4 mM (B). $[\text{Mg}^{2+}]_{\text{ext}}$ was adjusted to keep the total divalent cation concentration constant (4 mM). Whilst F_m measured at the end of a 100-Hz AP train was not affected by changing $[\text{Ca}^{2+}]_{\text{ext}}$, both the amplitude ΔF of Fluo-4 responses to a single AP and the rate of rise in fluorescence during 100-Hz stimulation were increased at higher $[\text{Ca}^{2+}]_{\text{ext}}$. (C, D) Fractional change of peak AP-evoked fluorescence response was similar in all recorded boutons irrespective of the initial $\Delta F/F_m$ value when $[\text{Ca}^{2+}]_{\text{ext}}$ was changed from 1 mM to 2 mM (C, $n=24$ boutons from four axons) or from 2 mM to 4 mM (D, $n=21$ bouton from five axons). Dashed lines $y=1.33 \times (C)$ and $y=1.38 \times (D)$. doi:10.1371/journal.pbio.1001396.g007

release-ready vesicles which, in turn, is related to the AZ size and the presynaptic bouton volume [8,13,15,16,55]. By measuring exocytosis and Ca^{2+} signaling concurrently, and by dissecting RRP and p_v at individual boutons, we have identified a second major determinant of different release probabilities among synapses: the average fusion probability of individual RRP vesicles p_v . Our data argue that p_v varies as a direct consequence of inter-synaptic differences of AP-evoked presynaptic Ca^{2+} influx independently of RRP and synaptic bouton size. Both sources of variability, RRP and p_v contribute approximately equally to the overall variability of P_{rel} among synapses supplied by the same axon.

Current understanding of the quantitative relationship between presynaptic Ca^{2+} entry and neurotransmitter release relies mostly on studies of individual large or giant synapses, such as those made by hippocampal mossy fibers or the Calyx of Held [36,56,57], which can be patch-clamped to control the presynaptic membrane potential and to manipulate or measure Ca^{2+} concentrations. However, the overwhelming majority of synapses in the CNS are too small ($\sim 1 \mu\text{m}$ scale) to permit such approaches, and therefore until now, the Ca^{2+} dependency of neurotransmitter release in small synaptic boutons could only be assessed at the population level, thus obscuring the determinants of heterogeneity (for review see [30,58,59]). We have overcome this barrier by combining imaging of vesicular exocytosis with measurements of presynaptic Ca^{2+} dynamics at the same small boutons.

To compare the efficacy of AP-evoked vesicular release among synapses supplied by a given axon we modified the classical FM-dye imaging approach and simultaneously measured, at the level of single boutons, all the major determinants of AP-evoked vesicular release including RRP size, the average fusion probability of individual RRP vesicles p_v , and the overall AP-evoked vesicular release rate R_{rel} . It should be noted that whilst R_{rel} is directly proportional to the average number of vesicles released in response to a single AP (N_{AP}), it is not exactly the same as a common interpretation of P_{rel} , which is the probability that at least one vesicle is released during a single AP. Because $P_{rel} = 1 - (1 - p_v)^{RRP}$, it follows that $N_{AP} > P_{rel}$ unless p_v is small [8,41]. However, because in our dataset average $p_v = 0.04$ (Figure 3), and the RRP in cultured hippocampal neurons contains on average five to seven vesicles [12,13], we estimate that the average values for $N_{AP} = 0.24$ and $P_{rel} = 0.22$ were indeed similar.

The methodological advances reported here include not only the first simultaneous measurements of RRP size and p_v at small synapses supplied by a single axon, but also a validation of the use of the high-affinity Ca^{2+} indicator Fluo-4 for an unbiased read-out of presynaptic Ca^{2+} dynamics. It has been previously shown that Ca^{2+} fluorescence decay time constants (which are thought to be proportional to the endogenous Ca^{2+} buffering capacity) can vary among putative synaptic boutons in the neocortex [20] or in the cerebellum [49]. However, we did not find any significant differences in the time-course of AP-evoked Ca^{2+} fluorescence transients measured with the high affinity Ca^{2+} indicator Fluo-4 in boutons supplied by single axons of cultured hippocampal neurons. This argues that inter-bouton variability of $\Delta F/F_m$ signals observed in our experiments cannot be simply explained by differences in endogenous Ca^{2+} buffers. Indeed, a non-stationary single-compartment model of presynaptic Ca^{2+} dynamics predicts that, whilst endogenous Ca^{2+} buffers should substantially affect the kinetics of AP-evoked Ca^{2+} fluorescence transients, they should exert only limited effects on peak $\Delta F/F_m$ values (Figure 6). This at a first sight unexpected result can be explained if one bears in mind that the Ca^{2+} association rate of the fast BAPTA-based Ca^{2+} fluorescent dye Fluo-4 is 10–30-fold higher than that of the major endogenous Ca^{2+} buffers such as parvalbumin and calbindin- $\text{D}_{28\text{K}}$ (Table S1). Therefore Ca^{2+} ions entering presynaptic bouton during an AP should first bind to the fast Ca^{2+} indicator Fluo-4 and only then to the slower acting buffers such as calbindin- $\text{D}_{28\text{K}}$ or parvalbumin. This also explains deviation of AP-evoked Ca^{2+} fluorescence profiles from the monoexponential kinetics predicted by a classical steady-state model [46–49], arguing against the common assumption that endogenous Ca^{2+} buffers uniformly slow down the decay of AP-evoked Ca^{2+} fluorescence transients. In fact, we find that endogenous buffers first accelerate and then slow down the AP-evoked Ca^{2+} fluorescence kinetics (Figure 6A and 6C).

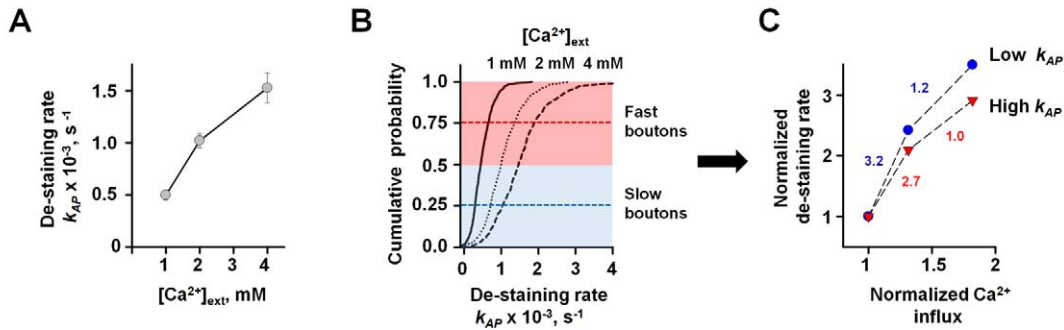


Figure 8. Inter-synaptic variability of Ca^{2+} cooperativity of AP-evoked vesicular release. (A) Dependency of the average AP-evoked de-staining rate k_{AP} on $[Ca^{2+}]_{ext}$. Data are mean \pm SEM from six independent experiments for each $[Ca^{2+}]_{ext}$. (B) Cumulative distributions of k_{AP} at different $[Ca^{2+}]_{ext}$ (1 mM, 620 boutons; 2 mM, 550 boutons, and 4 mM, 555 boutons). (C) Ca^{2+} cooperativity of vesicular release is higher in boutons with slow SRC1 de-staining (blue) than in boutons with fast SRC1 de-staining (red): k_{AP} values at different $[Ca^{2+}]_{ext}$ corresponding to cumulative probabilities 0.75 (Fast boutons) and 0.25 (Slow boutons) were normalized to the corresponding de-staining rates at 1 mM $[Ca^{2+}]_{ext}$ and then plotted against the relative amplitude of Ca^{2+} influx (determined as in Figure 7), which was also normalized to its value at 1 mM $[Ca^{2+}]_{ext}$. Numbers next to the dotted lines connecting the data points correspond to differential Ca^{2+} cooperativity of vesicular release calculated using the equation $m = \Delta \log(k_{AP}) / \Delta \log(\Delta[Ca^{2+}]_{total})$ [63] (blue, slow boutons; red, fast boutons). doi:10.1371/journal.pbio.1001396.g008

Another interesting prediction from the non-stationary analysis was that $\Delta F/F_m$ should give a linear readout of the total magnitude of the AP-evoked presynaptic Ca^{2+} influx $\Delta[Ca^{2+}]_{total}$ (providing that $\Delta F/F_m < 0.5 - 0.6$) (Figure S7). Again, at a first sight this was unexpected, because it is commonly thought that high affinity Ca^{2+} indicators (e.g., Fluo-4) do not linearly report AP-evoked changes in presynaptic Ca^{2+} concentration. This is indeed the case when one considers changes in the free cytosolic Ca^{2+} concentration $\Delta[Ca^{2+}]_{free}$ [20,22,49]. However, the total AP-evoked change of in presynaptic Ca^{2+} concentration also includes changes in the concentration of Ca^{2+} bound to Fluo-4 and Ca^{2+} bound to endogenous Ca^{2+} buffers: $\Delta[Ca^{2+}]_{total} = \Delta[Ca^{2+}]_{free} + \Delta[Ca^{2+}]_{Fluo-4} + \Delta[Ca^{2+}]_{Buf}$. The model then predicts that, when the total intracellular concentration of Fluo-4 is sufficiently high, a large part of the Ca^{2+} entering the nerve terminal during an AP should bind to the indicator (Figure S7, $\Delta[Ca^{2+}]_{free} / \Delta[Ca^{2+}]_{total} < 100$), and therefore that $\Delta[Ca^{2+}]_{total}$ should be proportional to $\Delta F/F_m$. In full agreement with this prediction we found that $\Delta F/F_m$ was indeed proportional to $\Delta[Ca^{2+}]_{total}$ when we manipulated extracellular $[Ca^{2+}]$ (Figure 7).

Importantly, the above results argue that the major experimental paradigm used here (where SRC1 measurements of vesicular release were performed prior to Fluo-4 loading) provides an unbiased comparison of Ca^{2+} -exocytosis coupling among individual boutons supplied by a given axon. Indeed whilst the absolute $\Delta F/F_m$ value in each experiment does depend on the total intraterminal concentration of Fluo-4, the intracellular loading of Fluo-4 does not affect the AP-evoked Ca^{2+} influx itself. Furthermore, because the Fluo-4 concentration was the same in all boutons supplied by the same axon (Figure S5), and because $\Delta F/F_m$ was proportional to $\Delta[Ca^{2+}]_{total}$, inter-synaptic differences in $\Delta F/F_m$ should be proportional to differences in $\Delta[Ca^{2+}]_{total}$ that would have been observed even in the absence of Fluo-4.

The strong correlation between $\Delta F/F_m$ and vesicular release rates further argues that conventional fluorescence measurements of volume-averaged presynaptic Ca^{2+} transients provide a faithful gauge of the vesicular release probability, at least within a homologous population of synapses. Indeed, the predominant location of presynaptic VGCCs at the AZ [31–35] suggests that $\Delta F/F_m$ should be determined mainly by Ca^{2+} influx at the AZ. On

the other hand the total number of Ca^{2+} ions entering a presynaptic terminal during an AP is proportional to $\Delta F/F_m$ and to the bouton volume: $N_{Ca} \propto \Delta F/F_m \cdot V$. Then, by bearing in mind that in general the size of the RRP is proportional to the bouton volume ($RRP \propto V$) (Figure 5A) [12], we infer that the average magnitude of AP-evoked Ca^{2+} influx calculated per single docked vesicle (N_{Ca}/RRP) should be directly proportional to the AP-evoked Ca^{2+} fluorescence signal: $N_{Ca}/RRP \propto \Delta F/F_m$. In full agreement with this prediction we found that the Ca^{2+} cooperativity of vesicular release was significantly lower in synaptic boutons with high p_v (Figure 8), which points to relative saturation of the Ca^{2+} vesicular release sensor due to higher Ca^{2+} influx at the AZ.

Our main finding is that both R_{rel} and p_v co-vary with the AP-evoked Ca^{2+} fluorescence response $\Delta F/F_m$, arguing that inter-synaptic variability of presynaptic Ca^{2+} dynamics is a major determinant of bouton to bouton differences in synaptic efficacy. Vesicular release probability may also be regulated by other factors such as small differences in endogenous Ca^{2+} buffering, which could not be detected with high concentrations of Fluo-4, or differences in the coupling distance between VGCCs and Ca^{2+} sensors for exocytosis [39]. However, if these factors play an important role in setting the basal p_v in a particular neuron they are unlikely to do so differentially at the level of individual boutons supplied by a given axon, because such variability would be expected to disrupt the tight correlation observed between p_v and $\Delta F/F_m$ in the present study.

What are the possible mechanisms that could account for the heterogeneity of Ca^{2+} influx? AP-dependent release at small hippocampal synapses is triggered by mixed populations of P/Q- and N-type VGCCs that have been proposed to saturate specific presynaptic ‘‘slots’’ [37,38] (although see [39]). These hypothetical VGCC slots put a limit on the number of VGCCs that can trigger release of docked vesicles in the RRP. Indeed, opening of three or fewer P/Q-type VGCCs appears to be sufficient to trigger release at GABAergic hippocampal synapses [60]. Moreover, the recent finding that RIM proteins specifically tether P/Q- and N-type channels to the AZ provides a possible mechanism for the molecular organization of such VGCC-specific slots [34,35]. This raises the possibility that the average number of presynaptic slots (and as a consequence the number of active VGCCs) surrounding

vesicles in the RRP might vary among presynaptic boutons located on the same axon. According to this model, the number of VGCCs per RRP vesicle would provide a straightforward mechanism for direct regulation of p_v . An alternative hypothesis is that heterogeneity in Ca^{2+} influx reflects systematic differences in the probability of VGCC opening during an AP potential or in the Ca^{2+} flux via individual channels. This in turn could be caused by several factors including inter-synaptic differences in the AP shape, differences in the type-specific composition of presynaptic VGCC mix [61], differential regulation of VGCC by G-proteins [62] or by auxiliary subunits [39]. However, which of these factors account for the variability of presynaptic Ca^{2+} influx cannot be determined at present.

Parallel regulation of AP-evoked vesicular release by RRP size and by Ca^{2+} -dependent scaling of p_v has important physiological implications, because it potentially allows the basal strength of synaptic transmission to be dissociated from short-term synaptic plasticity. For instance, during a train of presynaptic APs, boutons with a high basal p_v should exhibit more use-dependent depression because of depletion of the RRP, and/or attenuated facilitation because of saturation of the Ca^{2+} sensor for exocytosis. Conversely, if p_v were similar at boutons of different size, and therefore different RRP size, synapses with high and low basal release probability should exhibit similar short term plasticity (assuming, that is, that vesicles in the RRP fuse independently of one another). Furthermore, Ca^{2+} -dependent regulation of p_v should also allow synapse-specific modulation of neurotransmitter release that depends on changes in AP-evoked presynaptic Ca^{2+} influx: stronger saturation of the Ca^{2+} sensor for exocytosis in boutons with high p_v should make vesicular release in these synapses less sensitive to changes in presynaptic Ca^{2+} influx, due for example to modulation of VGCCs by G-proteins. Thus our data argue that inter-synaptic variability of Ca^{2+} influx provides a direct mechanism for the regulation and use-dependent redistribution of synaptic strengths across populations of small central synapses.

Methods

Cell Cultures and Imaging Solutions

Hippocampal neurons were isolated from P0–P2 rat pups [14] and cultured in Neurobasal based medium on an astrocyte feeder layer. All experiments were conducted at ambient temperature (23°C to 26°C) 13–19 d after plating. The imaging solution contained (in mM) 125 NaCl, 2.5 KCl, 2 MgCl_2 , 2 CaCl_2 , 30 glucose, and 25 HEPES (pH 7.4). To avoid recurrent activity synaptic transmission was blocked by supplementing the imaging solution with (in μM) 10 NBQX (Ascent Scientific), 50 DL-AP5 (Ascent Scientific), and 100 Picrotoxin (Tocris Bioscience).

Fluorescence Set-Up

Fluorescence imaging experiments were performed on an inverted LSM 510 confocal microscope (Zeiss) using a $63\times$ (1.4 NA) oil immersion objective. Fluo-4 and SRC1 were simultaneously excited using the 488-nm line of an argon laser and emissions were recorded using band pass 505–550-nm and long pass 585-nm filters, respectively. Alexa Fluor 568 was excited by a 543-nm He-Ne laser and its emission was recorded using a band pass 560–615-nm filter. Cross-talk between the fluorescence channels was less than 5%.

Imaging of Vesicular Release

To image AP-evoked vesicular exocytosis all recycling vesicles were labeled with the low affinity red fluorescence styryl dye SRC1 (SynaptoRed C1, Biotium) (at a bath concentration of 200 μM) using

several round of exhaustive high-frequency stimulation (four trains of 120 APs at 30 Hz delivered at 20-s intervals) followed by dye washout for 15 min with the imaging solution. APs were evoked by field stimulation via platinum bath electrodes separated by 1 cm (12.5–15 V, 1-ms pulses). The SRC1 fluorescence decay during high- and low-frequency stimulations was recorded as detailed in experimental paradigms (Figures 1A and 3A) in a $\sim 150\ \mu\text{m}\times 150\ \mu\text{m}$ region of interest (ROI; $1,024\times 1,024$ pixels) containing several hundred boutons. Background fluorescence in the SRC1 channel was determined by applying three rounds of high-frequency stimulation used for loading. The SRC1 photobleaching rate determined in control experiments was less than 0.2% per frame.

Images were analyzed using ImageJ (US National Institutes of Health). Following the X-Y alignment of recorded SRC1 consecutive images, active boutons were identified by subtracting a five-frame background average (acquired after the high-frequency de-staining stimulation protocol) from a five-frame average immediately after completion of SRC1 washout. To measure SRC1 de-staining kinetics in individual synaptic boutons fluorescence intensity was obtained from ROIs centered at the fluorescence maxima of individual boutons that completely covered the bouton area (characteristic linear dimensions ~ 1.0 – $2.0\ \mu\text{m}$). Boutons with overlapping ROIs were excluded from the analysis. The spontaneous (k_{sp}) and AP-evoked (k_{ev}) de-staining rates were calculated by fitting mono-exponential functions to the fluorescence time course in each selected ROI, after subtracting the background value. The specific AP-evoked SRC1 de-staining rate was calculated as $k_{AP} = k_{ev} - k_{sp}$. Boutons with high spontaneous de-staining rate ($k_{sp} > 0.005\ \text{s}^{-1}$) and boutons with low signal to noise ratio (goodness of the fit $\chi^2 > 0.0025$) were excluded from the analysis. The size of the TRP of vesicles was estimated as proportional to the total specific fluorescence loss in each ROI: $TRP \sim \Delta F_{FMtotal} = F_{FM_Load} - F_{FM_Background}$ (where F_{FM_Load} is a five-frame average of SRC1 fluorescence immediately after completion of SRC1 washout and $F_{FM_Background}$ is a five-frame background average acquired after the high-frequency de-staining stimulation protocol). The size of the RRP of vesicles was estimated as proportional to the total fluorescence loss triggered by a 30-Hz train of 60 APs: $RRP \sim \Delta F(60AP)/\varphi = [F_{FM_before} - F_{FM_after}]/\varphi$ (where F_{FM_before} and F_{FM_after} are SRC1 fluorescence measured immediately before and after the train and $\varphi = 2.74$ is a scaling factor determined as detailed in Text S2).

Imaging of Presynaptic Ca^{2+} Dynamics

For presynaptic Ca^{2+} imaging the selected neuron was loaded, via a whole-cell pipette, with 200 μM Fluo-4 and 200 μM Alexa Fluor 568 in a solution containing (mM): 135 KMS, 10 HEPES, 10 Na-phosphocreatine, 4 MgCl_2 , 4 $\text{Na}_2\text{-ATP}$, 0.4 Na GTP. After breaking in, the fluorescence in the soma and the apical dendrites equilibrated within 5 min and the patch pipette was slowly withdrawn to minimize cytosol dialysis. Experiments were terminated if the resting membrane potential was above $-55\ \text{mV}$, or if the gigaseal was lost during pipette withdrawal. The dyes were allowed to equilibrate throughout the neuron for 40–50 min after retracting the patch pipette (Figure S5A and S5B), before Ca^{2+} fluorescence recordings were started. Fluorescence transients in identified boutons were recorded in fast line-scan mode ($\sim 500\ \text{Hz}$). Neurons were first stimulated using field electrodes with either a single pulse (five trials for each bouton) (Figures 1 and 7) or with five pulses at 0.5 Hz (Figure 4) to determine the magnitude of AP-evoked presynaptic Ca^{2+} transients, and then by a burst of high-frequency stimulation

(100 APs at 100 Hz) to determine the maximal fluorescence of saturated Fluo-4 [21,22,25]. After averaging of five individual trials and subtracting the background fluorescence in the Fluo-4 channel (which was determined outside of the path-loaded neuron) the amplitude of AP-evoked Ca^{2+} fluorescence responses in each bouton $\Delta F/F_m$ was calculated as outlined in Figure 1G. The relative bouton sizes (cytosol volume V) were estimated by calculating the specific Alexa Fluor 568 fluorescence in the corresponding ROIs as outlined in Figure S5C.

Supporting Information

Figure S1 Properties of SRC1 de-staining in individual synaptic boutons during low-frequency stimulation. (A–E) Distribution of SRC1 de-staining parameters recorded in individual boutons (309 boutons from five independent experiments). (A) De-staining rate in the absence of stimulation, k_{sp} ; (B) de-staining rate during 0.5-Hz stimulation, k_{ev} ; (C) Specific AP-evoked de-staining rate $k_{AP} = k_{ev} - k_{sp}$; (D) Relative size of recycling pool of vesicles, calculated as $TRP_{REL} = \Delta F_{FMtotal}$ (RFU, relative fluorescence units); (E) Vesicular release rate, $R_{rel} = [k_{AP} \cdot \Delta F_{FMtotal}] / \nu$ ($\nu = 0.5$ Hz, stimulation frequency). (F) The AP-evoked de-staining rate k_{AP} does not depend on the TRP size. Correlation coefficient ρ and significance level p (Spearman rank correlation test) are indicated. (G–I) Specific SRC1 de-staining rates calculated per AP are the same during 0.25-Hz and 0.5-Hz stimulation. (G) Average de-staining profiles from two typical experiments at 0.5-Hz and 0.25-Hz stimulation. Distributions of AP-evoked SRC1 de-staining rates at 0.5 Hz (black, 410 boutons from four experiments) and at 0.25 Hz (gray, 544 boutons from four experiments) calculated per second (H) or per AP (I). The absolute AP-evoked SRC1 de-staining rate was lower during 0.25-Hz stimulation (H), whilst the specific SRC1 de-staining rate calculated per AP had the same distribution at 0.25 Hz and 0.5 Hz (I), $p = 0.28$, Kolmogorov-Smirnov test. (TIF)

Figure S2 Co-variation of vesicular release rate and AP-evoked presynaptic Ca^{2+} fluorescence transient: raw data from single axons. Dependencies of AP-evoked SRC1 de-staining rate k_{AP} (top row) and vesicular release rate R_{rel} (bottom row) on the amplitude of AP-evoked presynaptic Ca^{2+} fluorescence $\Delta F/F_m$ in five axons measured in five independent experiments. SRC1 measurements were performed prior to Fluo-4 loading (experimental protocol as in Figure 1, pooled normalized data are shown in Figure 2). Spearman rank correlation coefficients ρ are indicated. Dashed lines show data fits with a power function $y = a \cdot x^m$. (TIF)

Figure S3 Verification of the protocol for estimating of RRP/TRP ratio with short high-frequency stimulation bursts (related to Text S2). (A) Experimental paradigm. After SRC1 loading and washout relative SRC1 fluorescence losses in individual boutons were determined after two trains of 30-Hz stimulation separated by a 7.5-s interval. (B) Example traces recorded in individual boutons using different stimulations protocols. (C) Dependency of the ratio $\Delta FM(N APs) / \Delta FM(60 APs)$ between average SRC1 fluorescence losses after the test train (consisting of n APs) and control train (consisting of 60 APs) on the number of APs in the test train. Dashed line represents a least square data fit using Equation 2.5 from Text S2. Data are mean \pm SEM from 150–300 individual boutons from four independent experiments for each condition. (TIF)

Figure S4 Comparison of functional vesicular pool sizes in synapses supplied by single axons. (A–C) Left panels, frequency histograms of: (A) relative TRP size calculated as total specific loss of SRC1 fluorescence during de-staining experiment: $TRP_{REL} = \Delta F_{FMtotal}$, (B) relative RRP size calculated as the specific fluorescence loss stimulated by a 2-s 30-Hz stimulation divided by the scaling coefficient $\phi = 2.74$ (see Text S2) $RRP_{REL} = \Delta FM(60 APs) / 2.74$, and (C) relative vesicular release rate R_{rel} calculated as $R_{rel} = \Delta F_{FMtotal} \cdot k_{AP}$ from the experiment illustrated in (Figure 3). Blue histogram, boutons supplied by the Alexa loaded axon; gray histogram, all boutons in the field of view. (A–C) Right panels, summary data for variability of: (A) TRP size, (B) RRP size, and (C) R_{rel} . Blue bars, average CVs for synaptic boutons located on single axons; grey bars, average CVs for all boutons recorded in the same experiments. Data are mean \pm SEM from 11 independent experiments. (D, E). RRP size scales linearly with the TRP size: relationships between RRP and TRP (D) and between RRP/TRP and TRP (E). (F, G) AP-evoked SRC1 de-staining rate k_{AP} does not depend on the RRP size (F) or on the TRP size (G). Data in (D–G) are from the same experiment as illustrated in Figure 3. Blue, data points from boutons supplied by the Alexa loaded axon; grey data points from all boutons in the field of view. Dotted lines in (D–G) show linear regression for all data points. Correlation coefficients ρ and significance levels p (Spearman rank correlation test) are indicated. (TIF)

Figure S5 Patch-loading of synaptic boutons with the Ca^{2+} indicator Fluo-4 and the fluorescent morphological tracer Alexa Fluor 568 and measurements of synaptic bouton size. (A) Fluorescence image of a typical cultured hippocampal neuron 45 min after the beginning of patch-loading with Alexa Fluor 568 and Fluo-4. Note that the patch pipette was withdrawn within 5 min to minimize cytosol dialysis (Methods). The Alexa channel is shown in red, the Fluo-4 channel is not shown, and a reconstructed axon is shown in yellow. Inserts illustrate fluorescence images recorded in axonal boutons located at different distances from the soma (white boxes, ROIs 1, 2, and 3) at 5 min, 15 min, and 45 min after establishing of the whole-cell recording. Scale bars: main figure 20 μm , inserts 2 μm . (B) Time course of Alexa Fluor 568 fluorescence in the selected ROIs from (A). The gray box highlights the interval of the patch-loading (5 min). Since Fluo-4 and Alexa Fluor 568 have indistinguishable intracellular diffusion rates [21] we used Alexa Fluor 568 fluorescence to estimate the time-course of axonal loading for both Alexa Fluor 568 and Fluo-4. Because of diffusional redistribution of the dyes, the fluorescence time-course varied among boutons located at different distances from the soma. After 40 min Alexa Fluor 568 fluorescence stabilized throughout the neuron (up to 600 μm from the cell body). At this time point fluorescence in the soma was 70%–80% of its value at the moment of pipette withdrawal. Therefore, the actual concentrations of the fluorescent dyes in synaptic boutons were $\sim 25\%$ lower than those in the patch-pipette (i.e., $\sim 150 \mu\text{M}$). In the conditions of our experiments, photobleaching of Alexa Fluor 568 was negligible (less than 1% over 25 frames). (C, D) Estimation of bouton volume using Alexa Fluor 568. Cytosolic bouton volume should be proportional to the total specific Alexa Fluor 568 fluorescence F_{alexa} . To determine F_{alexa} , we integrated Alexa Fluor 568 fluorescence in a ROI that completely covers the bouton of interest (C, left panel) and then subtracted the integral background value corresponding to the same ROI. Importantly this estimate of F_{alexa} does not depend on the exact ROI size and shape, providing that it completely covers the synaptic bouton: (D) rectangular ROIs of increasing size (top) and dependency of the specific integral Alexa

Fluor 568 fluorescence on the ROI number, dashed line corresponds to F_{alexa} estimated in (C). Scale bar 2 μm . (TIF)

Figure S6 Comparison of AP-evoked Ca^{2+} fluorescence transients among boutons supplied by single axon. (A) Superimposed original traces showing variability of $\Delta F/F_m$ among boutons recorded in two different axon (five boutons in each experiment). (B) Scaled responses from the same boutons showing similar fluorescence decay rates in boutons from the same axon (average scaled traces are shown in black). (TIF)

Figure S7 Non-stationary single compartment model predicts linear relationship between $\Delta F/F_m$ and $\Delta[\text{Ca}^{2+}]_{total}$ when $0 < \Delta F/F_m < 0.6$. Theoretical relationships between AP-evoked peak fluorescence $\Delta F/F_m$ and total magnitude of volume averaged presynaptic Ca^{2+} influx $\Delta[\text{Ca}^{2+}]_{total}$ (left panels) and between change of free intracellular Ca^{2+} concentration $\Delta[\text{Ca}^{2+}]_{free}$ and $\Delta[\text{Ca}^{2+}]_{total}$ (right panels) in the absence of any endogenous buffers (A) and in the presence of 150 μM Calbindin- $\text{D}_{28\text{K}}$ (B) or 150 μM Parvalbumin (C). Fluorescence traces at in different conditions were calculated as described in the Text S3. To match the experimental data analysis $\Delta F/F_m$ values were obtained by averaging calculated fluorescence response over 10 ms interval immediately after the AP. $\Delta[\text{Ca}^{2+}]_{free}$ was calculated using
$$\Delta[\text{Ca}^{2+}]_{free} = \frac{\Delta F/F_m - 1/\gamma}{1 - \Delta F/F_m} - [\text{Ca}^{2+}]_0 \quad [22]$$
 where $\gamma = 100$ is the dynamic range of Fluo-4 and $[\text{Ca}^{2+}]_0 =$

0.05 μM is resting Ca^{2+} concentration used in simulations. This modeling predicts that in contrast to $\Delta[\text{Ca}^{2+}]_{free}$, $\Delta F/F_m$ (within the experimentally observed range ~ 0.1 – 0.6) should provide a linear readout of the total magnitude of volume averaged AP-evoked presynaptic Ca^{2+} influx $\Delta[\text{Ca}^{2+}]_{total}$. (TIF)

Table S1 Parameters used in the numerical non-stationary single compartment model. (PDF)

Text S1 Quantification of FM dye (SRC1) de-staining during low-frequency stimulation. (PDF)

Text S2 Measurements of RRP size with high-frequency stimulation. (PDF)

Text S3 Modeling presynaptic Ca^{2+} dynamics using non-stationary single compartment model. (PDF)

Author Contributions

The author(s) have made the following declarations about their contributions: Conceived and designed the experiments: KV DR DK. Performed the experiments: YE KV FA CH. Analyzed the data: KV YE. Wrote the paper: KV.

References

- Reyes A, Lujan R, Rozov A, Burnashev N, Somogyi P, et al. (1998) Target-cell-specific facilitation and depression in neocortical circuits. *Nat Neurosci* 1: 279–285.
- Koester H J, Johnston D (2005) Target cell-dependent normalization of transmitter release at neocortical synapses. *Science* 308: 863–866.
- Rozov A, Burnashev N, Sakmann B, Neher E (2001) Transmitter release modulation by intracellular Ca^{2+} buffers in facilitating and depressing nerve terminals of pyramidal cells in layer 2/3 of the rat neocortex indicates a target cell-specific difference in presynaptic calcium dynamics. *J Physiol* 531: 807–826.
- Mennerick S, Zorumski C F (1995) Paired-pulse modulation of fast excitatory synaptic currents in microcircuits of rat hippocampal neurons. *J Physiol* 488: 85–101.
- Markram H, Wang Y, Tsodyks M (1998) Differential signaling via the same axon of neocortical pyramidal neurons. *Proc Natl Acad Sci U S A* 95: 5323–5328.
- Scott R, Lalic T, Kullmann D M, Capogna M, Rusakov D A (2008) Target-cell specificity of kainate autoreceptor and Ca^{2+} -store-dependent short-term plasticity at hippocampal mossy fiber synapses. *J Neurosci* 28: 13139–13149.
- Dobrunz L E, Stevens C F (1997) Heterogeneity of release probability, facilitation, and depletion at central synapses. *Neuron* 18: 995–1008.
- Murthy V N, Sejnowski T J, Stevens C F (1997) Heterogeneous release properties of visualized individual hippocampal synapses. *Neuron* 18: 599–612.
- Slutsky I, Sadehpour S, Li B, Liu G (2004) Enhancement of synaptic plasticity through chronically reduced Ca^{2+} flux during uncorrelated activity. *Neuron* 44: 835–849.
- Branco T, Staras K, Darcy K J, Goda Y (2008) Local dendritic activity sets release probability at hippocampal synapses. *Neuron* 59: 475–485.
- Schikorski T, Stevens C F (2001) Morphological correlates of functionally defined synaptic vesicle populations. *Nat Neurosci* 4: 391–395.
- Schikorski T, Stevens C F (1997) Quantitative ultrastructural analysis of hippocampal excitatory synapses. *J Neurosci* 17: 5858–5867.
- Murthy V N, Schikorski T, Stevens C F, Zhu Y (2001) Inactivity produces increases in neurotransmitter release and synapse size. *Neuron* 32: 673–682.
- Waters J, Smith S J (2002) Vesicle pool partitioning influences presynaptic diversity and weighting in rat hippocampal synapses. *J Physiol* 541: 811–823.
- Branco T, Marra V, Staras K (2010) Examining size-strength relationships at hippocampal synapses using an ultrastructural measurement of synaptic release probability. *J Struct Biol* 172: 203–210.
- Holderith N, Lorincz A, Katona G, Rozsa B, Kulik A, et al. (2012) Release probability of hippocampal glutamatergic terminals scales with the size of the active zone. *Nat Neurosci* 15: 988–997.
- Gaffield M A, Betz W J (2006) Imaging synaptic vesicle exocytosis and endocytosis with FM dyes. *Nat Protoc* 1: 2916–2921.
- Ryan T A, Reuter H, Smith S J (1997) Optical detection of a quantal presynaptic membrane turnover. *Nature* 388: 478–482.
- Pyle J L, Kavalali E T, Piedras-Renteria E S, Tsien R W (2000) Rapid reuse of readily releasable pool vesicles at hippocampal synapses. *Neuron* 28: 221–231.
- Koester H J, Sakmann B (2000) Calcium dynamics associated with action potentials in single nerve terminals of pyramidal cells in layer 2/3 of the young rat neocortex. *J Physiol* 529 Pt 3: 625–646.
- Scott R, Rusakov D A (2006) Main determinants of presynaptic Ca^{2+} dynamics at individual mossy fiber-CA3 pyramidal cell synapses. *J Neurosci* 26: 7071–7081.
- Maravall M, Mainen Z F, Sabatini B L, Svoboda K (2000) Estimating intracellular calcium concentrations and buffering without wavelength ratioing. *Biophys J* 78: 2655–2667.
- Regehr W G, Atluri P P (1995) Calcium transients in cerebellar granule cell presynaptic terminals. *Biophys J* 68: 2156–2170.
- Sabatini B L, Regehr W G (1998) Optical measurement of presynaptic calcium currents. *Biophys J* 74: 1549–1563.
- Scott R, Ruiz A, Henneberger C, Kullmann D M, Rusakov D A (2008) Analog modulation of mossy fiber transmission is uncoupled from changes in presynaptic Ca^{2+} . *J Neurosci* 28: 7765–7773.
- Blatow M, Caputi A, Burnashev N, Monyer H, Rozov A (2003) Ca^{2+} buffer saturation underlies paired pulse facilitation in calbindin- $\text{D}_{28\text{k}}$ -containing terminals. *Neuron* 38: 79–88.
- Sara Y, Virmani T, Deak F, Liu X, Kavalali E T (2005) An isolated pool of vesicles recycles at rest and drives spontaneous neurotransmission. *Neuron* 45: 563–573.
- Lee S H, Rosenmund C, Schwaller B, Neher E (2000) Differences in Ca^{2+} -buffering properties between excitatory and inhibitory hippocampal neurons from the rat. *J Physiol* 525 Pt 2: 405–418.
- Sudhof T C (2004) The synaptic vesicle cycle. *Annu Rev Neurosci* 27: 509–547.
- Neher E, Sakaba T (2008) Multiple roles of calcium ions in the regulation of neurotransmitter release. *Neuron* 59: 861–872.
- Bucurenciu I, Kulik A, Schwaller B, Frotscher M, Jonas P (2008) Nanodomain coupling between Ca^{2+} channels and Ca^{2+} sensors promotes fast and efficient transmitter release at a cortical GABAergic synapse. *Neuron* 57: 536–545.
- Harlow M L, Ress D, Stoschek A, Marshall R M, McMahan U J (2001) The architecture of active zone material at the frog's neuromuscular junction. *Nature* 409: 479–484.
- Sun L, Li Q, Khanna R, Chan A W, Wong F, et al. (2006) Transmitter release face Ca^{2+} channel clusters persist at isolated presynaptic terminals. *Eur J Neurosci* 23: 1391–1396.

34. Kaeser P S , Deng L , Wang Y , Dulubova I , Liu X , et al. (2011) RIM proteins tether Ca(2+) channels to presynaptic active zones via a direct PDZ-domain interaction. *Cell* 144: 282–295.
35. Han Y , Kaeser P S , Sudhof T C , Schneggenburger R (2011) RIM determines Ca(2+) channel density and vesicle docking at the presynaptic active zone. *Neuron* 69: 304–316.
36. Sheng J , He L , Zheng H , Xue L , Luo F , Shin W , Sun T , Kuner T , Yue D T , Wu L G (2012) Calcium-channel number critically influences synaptic strength and plasticity at the active zone. *Nat Neurosci* 15: 998–1006.
37. Cao Y Q , Piedras-Renteria E S , Smith G B , Chen G , Harata N C , et al. (2004) Presynaptic Ca2+ channels compete for channel-type-preferring slots in altered neurotransmission arising from Ca2+ channelopathy. *Neuron* 43: 387–400.
38. Cao Y Q , Tsien R W (2010) Different relationship of N- and P/Q-type Ca2+ channels to channel-interacting slots in controlling neurotransmission at cultured hippocampal synapses. *J Neurosci* 30: 4536–4546.
39. Hoppa M B , Lana B , Margas W , Dolphin A C , Ryan T A (2012) α 2delta expression sets presynaptic calcium channel abundance and release probability. *Nature* 486: 122–125.
40. Oertner T G , Sabatini B L , Nimchinsky E A , Svoboda K (2002) Facilitation at single synapses probed with optical quantal analysis. *Nat Neurosci* 5: 657–664.
41. Christie J M , Jahr C E (2006) Multivesicular release at Schaffer collateral-CA1 hippocampal synapses. *J Neurosci* 26: 210–216.
42. Murthy V N , Stevens C F (1999) Reversal of synaptic vesicle docking at central synapses. *Nat Neurosci* 2: 503–507.
43. Stevens C F , Williams J H (2007) Discharge of the readily releasable pool with action potentials at hippocampal synapses. *J Neurophysiol* 98: 3221–3229.
44. Wesseling J F , Lo D C (2002) Limit on the role of activity in controlling the release-ready supply of synaptic vesicles. *J Neurosci* 22: 9708–9720.
45. Mozhayeva M G , Sara Y , Liu X , Kavalali E T (2002) Development of vesicle pools during maturation of hippocampal synapses. *J Neurosci* 22: 654–665.
46. Helmchen F , Borst J G , Sakmann B (1997) Calcium dynamics associated with a single action potential in a CNS presynaptic terminal. *Biophys J* 72: 1458–1471.
47. Neher E (1998) Usefulness and limitations of linear approximations to the understanding of Ca⁺⁺ signals. *Cell Calcium* 24: 345–357.
48. Jackson M B , Redman S J (2003) Calcium dynamics, buffering, and buffer saturation in the boutons of dentate granule-cell axons in the hilus. *J Neurosci* 23: 1612–1621.
49. Brenowitz S D , Regehr W G (2007) Reliability and heterogeneity of calcium signaling at single presynaptic boutons of cerebellar granule cells. *J Neurosci* 27: 7888–7898.
50. Muller A , Kukley M , Stausberg P , Beck H , Muller W , Dietrich D (2005) Endogenous Ca2+ buffer concentration and Ca2+ microdomains in hippocampal neurons. *J Neurosci* 25: 558–565.
51. Mochida S , Westenbroek R E , Yokoyama C T , Zhong H , Myers S J , Scheuer T , Itoh K , Catterall W A (2003) Requirement for the synaptic protein interaction site for reconstitution of synaptic transmission by P/Q-type calcium channels. *Proc Natl Acad Sci U S A* 100: 2819–2824.
52. Tottene A , Conti R , Fabbro A , Vecchia D , Shapovalova M , Santello M , van den Maagdenberg A M , Ferrari M D , Pietrobon D (2009) Enhanced excitatory transmission at cortical synapses as the basis for facilitated spreading depression in Ca(v)2.1 knockin migraine mice. *Neuron* 61: 762–773.
53. Raghavachari S , Lisman J E (2004) Properties of quantal transmission at CA1 synapses. *J Neurophysiol* 92: 2456–2467.
54. Stevens C F , Wang Y (1995) Facilitation and depression at single central synapses. *Neuron* 14: 795–802.
55. Kay L , Humphreys L , Eickholt B J , Burrone J (2011) Neuronal activity drives matching of pre- and postsynaptic function during synapse maturation. *Nat Neurosci* 14: 688–690.
56. Schneggenburger R , Forsythe I D (2006) The calyx of Held. *Cell Tissue Res* 326: 311–337.
57. Bischofberger J , Engel D , Frotscher M , Jonas P (2006) Timing and efficacy of transmitter release at mossy fiber synapses in the hippocampal network. *Pflügers Arch* 453: 361–372.
58. Eggermann E , Bucurenciu I , Goswami S P , Jonas P (2011) Nanodomain coupling between Ca(2+) channels and sensors of exocytosis at fast mammalian synapses. *Nat Rev Neurosci* 13: 7–21.
59. Branco T , Staras K (2009) The probability of neurotransmitter release: variability and feedback control at single synapses. *Nat Rev Neurosci* 10: 373–383.
60. Bucurenciu I , Bischofberger J , Jonas P (2010) A small number of open Ca2+ channels trigger transmitter release at a central GABAergic synapse. *Nat Neurosci* 13: 19–21.
61. Reid C A , Clements J D , Bekkers J M (1997) Nonuniform distribution of Ca2+ channel subtypes on presynaptic terminals of excitatory synapses in hippocampal cultures. *J Neurosci* 17: 2738–2745.
62. Scheuber A , Miles R , Poncer J C (2004) Presynaptic Cav2.1 and Cav2.2 differentially influence release dynamics at hippocampal excitatory synapses. *J Neurosci* 24: 10402–10409.
63. Matveev V , Bertram R , Sherman A (2009) Ca2+ current versus Ca2+ channel cooperativity of exocytosis. *J Neurosci* 29: 12196–12209.